ANL-7307
Reactor Technology
(TID-4500)
AEC Research and
Development Report

ARGONNE NATIONAL LABORATORY
9700 South Cass Avenue
Argonne, Illinois 60439

# MONTE CARLO ANALYSIS OF REACTIVITY COEFFICIENTS IN FAST REACTORS; GENERAL THEORY AND APPLICATIONS

by

Laurence B. Miller

Reactor Physics Division

Submitted in partial fulfillment of
the requirements for the degree of
Doctor of Philosophy in Nuclear Engineering
in the Graduate College of the
University of Illinois, 1967

March 1967

## DISCLAIMER

# TABLE OF CONTENTS

TABLE OF CONTENTS

## LIST OF FIGURES



## LIST OF TABLES

# MONTE CARLO ANALYSIS OF REACTIVITY COEFFICIENTS IN FAST REACTORS; GENERAL THEORY AND APPLICATIONS

by

Laurence B. Miller

## CHAPTER I
## INTRODUCTION

### A. The Problem in General

Recent design studies for fast power reactors[61,63,84,93] have pointed out the difficulty of achieving reactor stability. In each design, neutron economy had to be compromised in order to achieve a stable reactor system.

Although stability is a major consideration in the design of any reactor system, the difficulty is most acute in the design of a fast reactor. The mechanisms that contribute to power stability in thermal-reactor systems cannot be relied upon to provide the prompt negative temperature coefficient required in fast reactors, which have a much shorter neutron lifetime. The mechanisms of fuel expansion, low-energy spectrum shift, and coolant expansion are delayed by the time required for heat transfer, and are not, therefore, of primary importance in fast reactors. The effect of increased leakage with increasing temperature is important in small fast reactors. However, in reactors of the most economic size, with power levels of approximately 1000 MW, the surface-to-volume ratio is much smaller, and the leakage effect is not sufficiently large to guarantee reactor stability and safety. Therefore, the Doppler effect is of primary importance in establishing power stability in fast reactors. The ability to predict the Doppler coefficient in any proposed design is of the utmost importance, and all possible methods of increasing the magnitude of the Doppler effect must be understood. Techniques that accurately predict the Doppler coefficient in fast-reactor systems have been developed and are described here in detail. These techniques have been applied to investigate the possibility of increasing the Doppler coefficient by varying the size of the fuel elements while preserving the overall composition of the core. Particular emphasis has been placed upon eliminating certain approximations and assumptions that limit the accuracy and reliability of other current techniques.[41,56,60] The elimination of these approximations and assumptions, which was to make it possible to investigate the effect of fuel diameter on the Doppler coefficient, resulted in a more accurate technique for the analysis of the Doppler coefficient in fast reactors.

## B. Limitations of Current Theory

Shortly after Breit and Wigner[14] suggested that neutron cross sections as a function of energy could be represented by a formula similar to that for the natural shape of an optical line, Bethe and Placzek[11] discussed Doppler broadening of resonance cross sections due to thermal motion, and derived expressions for the temperature dependence of the cross sections, based on a Maxwell-Boltzmann distribution of nuclear velocities. These expressions, which are now universally used in the study of resonance absorption and its temperature dependence, are rigorously correct only for a monotomic gas. However, recent intensive studies[1] have shown that the error involved in using these expressions for a crystalline material is quite small, and these formulas remain as the basic analytic representation of temperature-dependent cross sections.

Wigner[95,98] first formulated the theory of resonance absorption in heterogeneous systems. His formulation was based upon the following assumptions:

1. The characteristics of a reactor can be studied by considering only a unit cell that is defined so that the reactor is composed of a number of such cells. Leakage can be ignored.

2. The collision density in the fuel is constant in lethargy (NR approximation).

3. The collision density in the moderator is constant in lethargy.

4. The neutron flux is independent of space in each material.

5. Scattering is isotropic in the laboratory system.

Chernick[20,21] introduced a more detailed formalism involving coupled integral equations for the collision densities in the moderator and the fuel. With this formalism he used either assumption 2 or the assumption:

6. The fuel resonances are narrow compared to the average energy loss in collisions with the moderator, but wide compared to that in collisions with the fuel (NRIA--narrow resonance-infinite mass absorber--approximation).

Corngold[24] eliminated assumption 4 by expanding the space- and angular-dependent flux in spherical harmonics. Unfortunately, the resulting formalism is quite unwieldy, and further work in this direction is discouraged by the formidable mathematics involved.

Because of the difficulty in obtaining a better approximation to the theory of resonance absorption by analytic techniques, recent work has been directed toward developing more exact numerical techniques. In 1963, Kier[55] developed a multigroup method for slab lattices which requires assumptions 1 and 5. He also assumed that:

7. Neutrons are scattered into the resonance region from a $1/E$ flux at higher energies.

Simultaneously, extending a technique developed by Nordheim[70] for homogeneous media, Lewis[60] developed a numerical-integration technique for a lattice of cylindrical fuel rods based on the same assumptions, but, in order to consider the commonly used cylindrical rods instead of flat plates, he required, in addition, the assumptions:

8. The unit cell can be approximated by a circular cell of the same volume.

9. The correct boundary condition for the circularized cell is: for each neutron leaving the cell, a neutron of the same energy enters the cell traveling in the opposite direction. Honeck[46] pointed out that the latter assumption is reasonably valid only for very large cells. He showed that a better approximation is:

10. For each neutron leaving the cell a neutron of the same energy enters the cell with all directions of travel equally probable.

Kier[56] developed a method for a two-region cell based upon this assumption and assumptions 1, 5, 7, and 8, as well as the assumption:

11. The flux-crossing boundaries between materials is isotropic. Also, the code is limited to considering resonance materials in the central region of the two-region circularized cell.

As Wigner[97] pointed out, neutron transport can be analyzed from two distinct points of view, analogous to the Lagrangian and Eulerian formulations of hydrodynamics. One can either consider the particle density in a unit volume of phase space, as particles continually enter and leave the volume, or one can focus attention on the individual particles and consider their motion through phase space. In the Lagrangian formulation of fluid mechanics, the particles are aggregates of many molecules, which can be considered to behave in a deterministic manner. However, in the formulation of neutron-transport theory, because of the more complex nature of the interactions, it is necessary to consider the motion of the individual neutrons and the probabilistic nature of their motion. One way to take this into account is to use sets of random numbers with frequency distributions

corresponding to the physical probabilities. The first serious attempt to solve neutron-transport problems in this way was by Fermi and Richtmyer[31] in Chicago and Ulam[92] in Los Alamos. Los Alamos gave the name Monte Carlo to the method in 1946. Development of the method was continued, notably, by Kahn,[48-52] Berger,[8,9] Albert,[2] and Goertzel and Kalos.[39] It was first used to solve resonance escape problems by Richtmyer, Van Norton, and Wolfe.[77] They developed the REP code,[78] which treats the slowing down of neutrons from a 1/E source in a rectangular cell, with a cylindrical fuel rod containing one resonance absorber. Dannels modified the code to treat a second resonance absorber.[4,27] His Repetitious III code is currently in use. Candelore and Gast[15] made a similar modification to produce the RECAP II code. However, the approximate expression,

$$\sigma = \sigma_0 \psi_0 \frac{1}{1 + (x\psi_0)^2}, \tag{1}$$

where

$$x = 2(E - E_0)/\Gamma, \tag{2}$$

$\Gamma$ = the total resonance width,

$E$ = neutron energy,

$E_0$ = energy of the resonance level,

$\psi_0 = \psi(x = 0, \theta)$,

$\psi$ = the Doppler line-shape function (defined by Eq. 25),

$4\theta$ = square of the ratio of the Doppler width to the natural width,

and

$\sigma_0$ = the unbroadened peak cross section,

is used to represent the cross sections of fuel materials in Repetitious III, and to represent the cross sections of all materials in the unresolved range in the RECAP II code.

If the expression

$$\frac{\psi_0}{1 + (x\psi_0)^2}, \tag{3}$$

is substituted for $\psi$ in the J integral, which is defined by

$$J = \int_0^\infty \frac{\psi}{\psi + \beta}\, dx, \tag{4}$$

where $\sigma_p$ is the potential scattering cross section, and

$$\beta = \sigma_p/\sigma_0,$$

we obtain

$$J = \frac{\pi}{2}\sqrt{\frac{1}{(\psi_0 + \beta)\beta}}. \tag{5}$$

Therefore, the use of the approximation to the cross section given by Eq. 1 would give, for the resonance integral of a narrow resonance,

$$I = \frac{\sigma_p}{E_0}\Gamma_a J = \frac{\pi}{2}\frac{\sigma_p}{E_0}\Gamma_a\sqrt{\frac{1}{(\psi_0 + \beta)\beta}}, \tag{6}$$

where

$$\Gamma_a = \Gamma_\gamma + \Gamma_f. \tag{7}$$

This can be expanded as follows for $\psi_0/\beta < 1$:

$$I = \frac{\pi}{2}\frac{\sigma_p}{E_0}\frac{\Gamma_a}{\beta}\left[1 - \frac{1}{2}\frac{\psi_0}{\beta} + \frac{3}{8}\frac{\psi_0^2}{\beta^2} - \ldots\right]. \tag{8}$$

In the region of interest, to first order in $\theta$,

$$\psi_0 \approx \sqrt{\frac{\pi}{2}}\,\frac{\theta}{\sqrt{2}}. \tag{9}$$

Therefore, using the approximate expression for $\sigma$ gives

$$I_{appr} = \frac{\pi}{2}\frac{\sigma_p}{E}\frac{\Gamma_a}{\beta}\left[1 - \left(\frac{1}{\beta}\sqrt{\frac{\pi}{2}}\frac{\theta}{2}\right)\frac{1}{\sqrt{2}} + \left(\frac{1}{\beta^2}\frac{\pi}{\sqrt{3}}\frac{\theta^2}{4}\right)\left(\frac{3}{8}\right)^{\frac{3}{2}} - \ldots\right]. \tag{10}$$

Using the correct expression for $\sigma$ gives[29]

$$I_{NR} = \frac{\pi}{2}\frac{\sigma_p}{E}\frac{\Gamma_a}{\beta}\left[1 - \left(\frac{1}{\beta}\sqrt{\frac{\pi}{2}}\frac{\theta}{2}\right) + \left(\frac{1}{\beta^2}\frac{\pi}{\sqrt{2}} + \frac{\theta^2}{4}\right) - \ldots\right]. \tag{11}$$

The second term of $I_{appr}$ is equal to the second term of $I_{NR}$ divided by $\sqrt{2}$. Therefore,

$$I_{appr} > I_{NR}. \tag{12}$$

Also,

$$\frac{\partial I_{appr}}{\partial \theta} \approx \frac{\partial I_{NR}}{\partial \theta} \cdot \frac{1}{\sqrt{2}},$$

or, since $\theta$ is directly proportional to the temperature, T,

$$\frac{\partial I_{appr}}{\partial T} \approx \frac{\partial I_{NR}}{\partial T} \cdot \frac{1}{\sqrt{2}}. \tag{13}$$

This implies that the capture rate in $Pu^{239}$ computed by Repetitious III is too high, and the temperature derivative of the capture rate is too low. If we compute the value of the second term in the brackets of Eq. 11,

$$\frac{1}{\beta}\sqrt{\frac{\pi}{2}}\frac{\theta}{2}, \tag{14}$$

using the average of the resonance parameters of $Pu^{239}$, we find that the error in the fission rate is only about 3% at 1 keV, but the error in the temperature derivative of the fission rate is about 40%.

Olhoeft[71] used these methods, together with a temperature-derivative estimator based on Albert's Neumann Series solution[2] of the Boltzmann equation, to investigate the effect of a nonuniform temperature distribution in reactor fuel elements on the Doppler coefficient. These Monte Carlo methods represented a distinct improvement over previous analytic and numerical techniques. However, they retained assumptions 1 and 7, and were further limited by insufficient accuracy in the computation of cross sections from the resonance parameters, excessive computing time requirements, and geometrical restrictions. The development of a complete algorithm based upon theories and techniques not dependent on the above assumptions and limitations was a major objective of the research described here.

## C. Scope of Research

Chapter II deals with the development of the general theory and techniques used in this research. Chapter III describes the incorporation of these techniques into a highly versatile computer program, the characteristics of the code that contribute to its accuracy and speed, and the numerous tests carried out to verify the accuracy and reliability of the code.

The ability of the code to accurately predict Doppler effects was checked by comparison with experiments carried out in critical facilities. The results of the comparisons, described in Chapter IV, verify the utility of the theory and techniques incorporated in the code.

Finally, computations were performed to determine the Doppler coefficient of a large fast-reactor system, and to investigate the possibility of increasing the Doppler coefficient by varying the fuel-rod diameter. Chapter V gives the computed value of the Doppler coefficient and conclusions concerning its variation with fuel-rod diameter.

Chapter VI discusses the applicability of the theory and techniques used in this research, describes some possible extensions of the present work, and, finally, summarizes general conclusions concerning the effect of fuel rod diameter on the Doppler coefficient.

# CHAPTER II

# MATHEMATICAL THEORY FOR SOLVING THE SPACE- AND ENERGY-DEPENDENT BOLTZMANN EQUATION BY INDIRECT ANALOGY

## A. General Background

### 1. Theory of Resonance Reactions

The study of nuclear-resonance phenomena began in the 1930's, following very closely in time and to some extent overlapping the development of the theory of atomic-resonance phenomena. Atomic-resonance theory was developed rapidly in the 1920's and 1930's by such authors as Henri, Teaves, Bonhoeffer, Wentzel, Kronig, Dirac, and Rice and the concepts evolved by their study were applied to nuclear-resonance phenomena by Bethe,[10] Fermi,[3] Moon and Tillman,[66] Beck and Horsley,[6] and Szilard[87] between 1930 and 1935. Breit and Wigner, in 1936, made a major contribution when they postulated the existence of quasi-stationary energy levels to account for the observed high-absorption cross sections without accompanying large scattering cross sections.[14] The theory was improved by Kapur and Peierls,[53] Bethe and Placzek,[11] Breit,[13] and Feshback, Peaslee, and Weisskopf.[32] Wigner and Eisenbud[96,99] and Teichmann[90] finally provided a treatment that took into account the strong nuclear interaction. Excellent summaries of their work are contained in books by Blatt and Weisskopf[12] and by Sachs.[82] The theory of resonance reactions is based on the concept of the compound nucleus. It has been inferred that a finite delay occurs between the time a neutron strikes a nucleus and the time the reaction products appear. During this time, the target nucleus plus the bombarding neutron exist as a single nucleus in an excited state, corresponding to a virtual energy level of the compound nucleus. The criterion for a reaction to take place is related to this delay time and to the existence of a virtual energy level of the compound nucleus at an energy corresponding to the energy of the ground state of the target nucleus plus the kinetic energy and binding energy of the neutron.

The virtual energy levels can be calculated from quantum-mechanical principles in exactly the same manner as bound energy levels are calculated. Experimentally, however, bound energy levels are identified by observing the energy of gamma rays emitted in transitions between bound states, while virtual energy levels are found from a study of the resonances observed when neutron cross sections are measured as a function of energy.

The observed virtual energy states are metastable, and the mean lifetime of the compound nucleus can be related to the width of the virtual energy level by Heisenberg's Uncertainty Principle,

$$\Delta E \, \Delta \tau = \frac{h}{2\pi}, \tag{15}$$

where

$\Delta E$ = energy,

$\Delta \tau$ = mean lifetime,

and

$h$ = Planck's constant.

Applied to the theory of resonance reactions, $\Delta E$ represents the width of the virtual energy level, which can be observed experimentally as the width at half-maximum (or the "half-width") of the resonance peaks on a plot of cross section vs incident neutron energy. Since the mean life of the compound nucleus, represented by $\Delta \tau$, is inversely proportional to the decay constant, $\lambda$, we can write

$$\Delta E = \lambda h / 2\pi. \tag{16}$$

The $\Delta E$ in this equation is usually denoted by $\Gamma$. If the compound nucleus is capable of disintegrating in several ways, a $\Gamma_i$ for each mode of decay is defined by

$$\Gamma_i = \lambda_i h / 2\pi. \tag{17}$$

Obviously,

$$\Gamma = \sum_i \Gamma_i. \tag{18}$$

The fact that the virtual energy levels of the compound nucleus have finite widths implies that the incident neutron need not have precisely the right amount of kinetic energy to form a compound nucleus at a precise energy of excitation. If the neutron energy is such as to produce a compound nucleus with an excitation energy within $\pm\frac{1}{2}\Gamma$ of the center of a virtual energy level, there is a high probability the reaction will take place. Since systems of subatomic particles exist stably only in discrete energy states, only neutrons and nuclei with appropriate relative velocities have a high probability of interacting. The interaction probability as a function of the total kinetic energy of the neutron and nucleus in the center of mass system, as given by the Breit-Wigner formula, is[14,30]

$$\sigma = \frac{\lambda^2}{4\pi} \frac{2I_c + 1}{(2I_n + 1)(2I + 1)} \frac{\Gamma_n \Gamma}{(E - E_0)^2 + (\Gamma/2)^2}, \tag{19}$$

where

$\lambda$ = deBroglie wavelength of the neutron,

$I_c$ = angular momentum of the compound nucleus,

$I_n$ = intrinsic angular momentum of the neutron,

$I$ = intrinsic angular momentum of the nucleus,

$\Gamma_n$ = neutron width of the excited level,

$\Gamma$ = total width of the excited level,

$E$ = kinetic energy of the neutron and the nucleus in the center of the mass system,

and

$E_0$ = excitation energy of the compound nucleus.

The interaction probability, or cross section, as a function of neutron velocity in the laboratory system, can be obtained by averaging the above function with the probability function for the velocity of the nuclei. The probability function for the velocity of the nuclei can be represented by the Maxwell-Boltzmann velocity distribution,[1,58]

$$P(V) = \frac{\exp[-V^2/4\theta]}{[4\pi\theta]^{3/2}}, \tag{20}$$

where

$$\theta = KT/2M, \tag{21}$$

$K$ = Boltzmann constant,

$T$ = temperature,

$M$ = mass of the nucleus,

and

$V$ = velocity of the nucleus.

If the nonresonance potential scattering is taken into account, the resulting expressions for the Doppler-broadened absorption and scattering cross sections are, respectively,[29]

$$\sigma_a = \sigma_0 \frac{\Gamma_\gamma}{\Gamma} \psi(\theta, x), \tag{22}$$

and

$$\sigma_s = \sigma_0 \frac{\Gamma_n}{\Gamma} \psi(\theta, x) + (\sigma_0 \sigma_p g \Gamma_n / \Gamma)^{1/2} \chi(\theta, x) + \sigma_p, \tag{23}$$

where

$$\sigma_0 = \frac{\lambda}{\pi} \frac{\Gamma_n}{\Gamma}, \tag{24}$$

$\Gamma_\gamma$ = radiation width,

$$\psi(\theta, x) = \frac{1}{\theta \cdot 2\sqrt{\pi}} \int_{-\infty}^{\infty} \frac{1}{1 + y^2} \exp\left[-\frac{(x - y)^2}{4\theta}\right] dy, \tag{25}$$

$$\chi(\theta, x) = \frac{1}{\theta \cdot 2\sqrt{\pi}} \int_{-\infty}^{\infty} \frac{y}{1 + y^2} \exp\left[-\frac{(x - y)^2}{4\theta}\right] dy, \tag{26}$$

$$x = 2(E - E_0)/\Gamma, \tag{27}$$

and

$$\theta = \frac{4KTE}{(M + 1)\ \Gamma^2}. \tag{28}$$

2. Theory of Stochastic Analysis

The method of stochastic analysis, when applied to neutron-transport problems is now commonly referred to as the Monte Carlo method. Briefly, the Monte Carlo method consists of following individual imaginary neutrons in their travel through space and energy, and using random numbers drawn from the appropriate probability distributions to determine the distances between collisions and the results of each collision. The collision points determined in this way constitute an unbiased sample which can be used to evaluate various integral functionals such as the absorption and fission rates. The theoretical basis of this method can be developed rigorously starting with a few well-established principles of the theory of statistical analysis.[36]

These concepts can be most easily explained in terms of the application of statistical analysis to the evaluation of integrals. Let S(X) be a function of X defined on the interval [a, b]. If we choose N sample values of S(X), corresponding to N values of X chosen randomly on the interval [a, b], we obtain an estimate for the mean of S(X) given by

$$\overline{S}_1 = \frac{1}{N} \sum_{i=1}^{N} S(X_i), \tag{29}$$

where $X_1, X_2, \ldots, X_N$ are the N randomly chosen values of X.

If we choose other sets of N sample values of S(X), we obtain other estimates of the mean, $\overline{S}_2, \overline{S}_3, \ldots$, etc. These estimates have a frequency distribution, called the sampling distribution. The sampling distribution has a mean, $\bar{\mu}$, and standard deviation, $\bar{\sigma}$. The mean, $\bar{\mu}$, is the same as the mean of S(X), and the standard deviation, $\bar{\sigma}$, is equal to $\sigma/\sqrt{N}$, where $\sigma$ is the standard deviation of S(X) from $\langle S(X) \rangle$. Thus $\overline{S}_1$ approximates $\langle S(X) \rangle$ more closely the larger the sample size.

These statistical results can be immediately applied to the evaluation of integrals, since

$$\int_a^b S(X)\, dX = \langle S(X) \rangle \cdot (b - a)$$

$$= \frac{1}{N} \sum_{i=1}^{N} S(X_i)(b - a) \pm \bar{\sigma}. \tag{30}$$

It is often advantageous to write the integral as

$$I = \int_a^b f(X)\, g(X)\, dX, \tag{31}$$

where $g(X) = S(X)/f(X)$, and f(X) is a convenient probability-distribution function.

This can be evaluated by choosing N values of X from the probability distribution

$$P(X) = \begin{cases} f(X)/c & a \leq X \leq b \\ 0 & X < a, \\ 0 & X > b \end{cases} \tag{32}$$

where c is the normalization constant such that

$$\int_a^b \frac{f(X)}{c}\, dX = 1. \tag{33}$$

The value of the integral is then

$$I = \frac{c}{N} \sum_{i=1}^{N} g(X_i). \tag{34}$$

The validity of Eq. 34 can be easily established. For $f(X) = 1$, $c = b - a$ and $g(X) = S(X)$, so Eq. 34 is identical to Eq. 30. Now suppose that $f(X)$ is such that $f(X_1) = F$. Then, the probability of $X_1$ being chosen from $P(X)$ is increased by the factor F. But, at the same time, $g(X_1) = S(X_1)/f(X_1)$ is decreased by the factor $1/F$. So the probable contribution of $g(X_i)$ to the sum of Eq. 34 is the same as in the case of $f(X) = 1$, and Eq. 34 is an unbiased estimator for the value of the integral I.

Now if we want to find the absorption probability for neutrons traversing a region of phase space, we can evaluate the absorption integral

$$I = \int_{\bar{a}}^{\bar{b}} \phi(\bar{X})\, \Sigma_a^z(\bar{X})\, d\bar{X} \tag{35}$$

by letting

$$f(\bar{X}) = \phi(\bar{X})\, \Sigma_t(\bar{X}) \tag{36}$$

and

$$g(\bar{X}) = \frac{\Sigma_a^z(\bar{X})}{\Sigma_t(\bar{X})}, \tag{37}$$

where

$\phi(\bar{X})$ = scalar flux,

$\Sigma_t(\bar{X})$ = total macroscopic cross section,

$\Sigma_a^z(\bar{X})$ = macroscopic absorption cross section of isotope z,

and

$\bar{X}$ = a point in six-dimensional phase space.

Here $f(\bar{X})$ is the collision density, and the points, $\bar{X}_i$, may be chosen from the probability distribution $p(\bar{X})$, by following individual neutrons through phase space and taking the successive collision points to be the points $\bar{X}_i$.

We have only to determine the normalization constant, c, such that

$$\int_{\bar{a}}^{\bar{b}} \phi(\bar{X})\, \Sigma_t(\bar{X})\, d\bar{X}/c = 1. \tag{38}$$

Since

$$\int_{\bar{a}}^{\bar{b}} \phi(\bar{X})\, \Sigma_t(\bar{X})\, d\bar{X} = N \tag{39}$$

is the total collision rate due to $N_s$ source neutrons per unit time entering the region under consideration, $c = N$. The value of the absorption integral is, explicitly,

$$I = \sum_{i=1}^{N} \frac{\Sigma_a^z(X_i)}{\Sigma_t(X_i)}, \tag{40}$$

and the absorption probability is $I/N_s$.

The first major consideration in any Monte Carlo calculation is the problem of choosing random numbers. One must be able to select numbers in such a way that the probability of choosing a given number, $\rho$, is proportional to some function of $\rho$, $f(\rho)$. For example, to determine the distance a neutron goes between one collision and the next, one must be able to choose random numbers in such a way that the probability of choosing a given number, $\rho_i$, is proportional to the probability of interaction at a distance $\rho$ from the initial point $\underline{X}$; i.e.,

$$f(\rho) = \Sigma(\underline{X} + \rho\underline{\Omega}) \exp\left[-\int_0^{\rho} \Sigma(\underline{X} + \rho'\underline{\Omega})\, d\rho'\right], \tag{41}$$

where $\Sigma$ is the total cross section and $\underline{\Omega}$ is the direction of travel.

This problem can be broken into two parts. The first part is generating random numbers uniformly distributed on the interval [0, 1]. The second part is using these numbers to obtain random numbers satisfying a given probability distribution.

The most common method of generating a series of random numbers on the interval [0, 1] is to multiply the preceding number in the series by a fixed multiplier, and to retain the least significant part of the product. For example, on a 40-bit computer,

$$\rho_{n+1} = 3^{24}\,\rho_n (\text{mod } 2^{39}) \tag{42}$$

is frequently used; i.e., we use a multiplier of $3^{24}$ and retain the least significant 40 bits. This is known as the multiplicative congruential method. Many other methods of generating pseudo-random number sequences have been used, but the multiplicative congruential method gives series that best satisfy the various tests for randomness.[47]

The techniques used to obtain random numbers satisfying a given probability distribution, utilizing a supply of random numbers uniformly distributed on the interval [0, 1] are very simple in theory, but ingenious in practice. Theoretically, one can obtain the random numbers, $X_i$, distributed according to the probability density function, f(X), from the relation

$$\int_0^{X_i} f(X)\,dX = \rho_i, \tag{43}$$

where the $\rho_i$ are random numbers uniformly distributed on the interval [0, 1]. This can be shown as follows.

Let $R(\rho)$ be the probability density function for the $\rho_i$; i.e., $R(\rho)\,\Delta\rho$ is the probability that $\rho_i$ will lie between $\rho$ and $\rho + \Delta\rho$. ($R(\rho) = 1$ for the uniform distribution [0, 1].) Define $X_i$ and $\Delta X$ by the relations

$$F(X_i) = \int_0^{X_i} f(X)\,dX = \rho_i \tag{44}$$

and

$$F(X_i + \Delta X) = \int_0^{X_i+\Delta X} f(X)\,dX = \rho_i + \Delta\rho, \tag{45}$$

where f(X) is an arbitrary positive definite function of X. Then,

$$F(X_i + \Delta X) - F(X_i) = \rho_i + \Delta\rho - \rho_i = \Delta\rho. \tag{46}$$

By Eqs. 44 and 45 and the fact that $F(X_i)$ is monotonic, there is an $X_i$ in the interval $[X, X + \Delta X]$ for each $\rho_i$ in the interval $[\rho, \rho + \Delta\rho]$. So if S(X) is the resultant probability distribution function for the $X_i$, then

$$S(X)\,\Delta X = R(\rho)\,\Delta\rho = \Delta\rho. \tag{47}$$

Combining Eqs. 46 and 47 and taking the limit as $\Delta X \to 0$, we have

$$\lim_{\Delta X \to 0} \frac{F(X_i + X) - F(X_i)}{\Delta X} = S(X), \tag{48}$$

or

$$\frac{dF}{dX} = S(X). \tag{49}$$

But from Eqs. 44 and 45,

$$\frac{dF}{dX} = f(X), \tag{50}$$

so that

$$S(X) \equiv f(X) \tag{51}$$

and the $X_i$ defined by Eq. 44 are distributed according to the probability distribution function $f(X)$.

For example, if the desired probability distribution is

$$f(X) = \cos X, \tag{52}$$

the random numbers $X_i$ can be obtained from uniformly distributed random numbers $\rho_i$ by using the relation

$$\int_0^{X_i} \cos X\, dX = \rho_i; \tag{53}$$

i.e., the $X_i$ with the desired distribution may be computed from

$$X_i = \arcsin \rho_i. \tag{54}$$

In practice, the evaluation of such transcendental functions is usually avoided by some ingenious use of random numbers. For example, should we need to compute the square root of a random number,

$$X_i = \sqrt{\rho_i}, \tag{55}$$

we would avoid the time-consuming process of extracting the square root, by obtaining two random numbers and choosing the maximum of the two to be $X_i$. This procedure is based on the previous theorem and on a modification of what is known as the "rejection technique."[44] Working backwards from the previous method, we see that if $X_i = \sqrt{\rho_i}$,

$$\rho_i = X_i^2, \tag{56}$$

and

$$\rho_i = \int_0^{X_i} 2X \, dX. \tag{57}$$

So the probability density function for the $X_i$ is $f(X) = 2X$, which, normalized to $1/2$ on its support, is

$$f(X) = X. \tag{58}$$

Now if we choose a tentative value for $X_i$ and accept this value only if a second random number is less than $f(X_i)$, the probability of accepting a given $X_i$ is proportional to $f(X)$. If we adopt this procedure, it might appear that we will have to reject one-half of the tentative values. But one final consideration shows this to be unnecessary. If we next interchange the role of the two random numbers, we note that one member of every pair of random numbers will be accepted--always the larger one. Whenever possible, such time-saving schemes are used in choosing from nonuniform probability distributions. If such a scheme cannot be found, Eq. 44 can always be used.

Having available a supply of random numbers distributed according to any desired probability distribution, we can follow individual neutrons in their flight from collision to collision. By tabulating the events that occur in the life of a sufficient number of neutrons, we can determine what actually occurs in a given physical system.

### 3. Techniques for Space Transport, Collision Mechanics, and Estimation of Probabilities

A Monte Carlo calculation can be set up in many ways to get the same result. For example, there are at least six alternate ways of treating space transport. The simplest approach is to carry out the calculation in direct analogy with the physical process. At each collision point, the neutron is either absorbed or scattered as determined by the selection of a random number. After each collision, the point of next collision is determined by the direction chosen from the appropriate probability distribution function and the distance, s, chosen from the relationship

$$\int_0^s \Sigma_t(x, E)\, ds = -\ln \rho. \tag{59}$$

The second possibility is similar to the first, except the distance between collisions is determined from the relationship

$$\int_0^s \Sigma_s(x, E)\, ds = -\ln \rho; \tag{60}$$

i.e., only scattering collisions are considered, and the absorption is calculated as

$$\int_0^s \Sigma_a e^{-\Sigma_t s}\, ds, \tag{61}$$

where s is the path length.

In the third method, the space transport is handled by a slight modification to the direct analog of the physical process, in which the neutron is allowed to continue without absorption at any collision and the neutron weight is adjusted as required to obtain the correct values for the absorption probability. This technique is discussed more fully in Chapter III.

A fourth possibility is the fractional interaction model, which will be described in detail in Section C of this chapter. In this model, the distance between collisions is determined from the relationship

$$s = \frac{-\ln \rho}{C(E)}, \tag{62}$$

where

$$C(E) = \text{supremum}\{\Sigma_t(\bar{X}, E') : E' = E\}; \tag{63}$$

i.e., C(E) is the largest cross section in the entire nuclear system at energy E. Then at each collision point the probability of an interaction that changes the speed and direction of the neutron is

$$\frac{\Sigma_t(\bar{X}, E)}{C(E)}. \tag{64}$$

The selection of a random number determines whether such a true interaction takes place at the collision point or whether the neutron continues

with its previous direction and speed. The advantage of this technique is that it eliminates the complicated procedures required to cross boundaries between different materials. Since it permits the determination of the next collision point without reference to the space dependence of the cross sections, it makes calculations on systems with extremely complex geometry practical. The validity of this method is proven in Section C of this chapter.

The fifth possibility is to permit the neutron to go exactly one mean free path between collisions and to adjust the neutron weight appropriately. This eliminates the need to evaluate $\ln \rho$ once for each collision. However, the validity of this approach has not been rigorously established.

A sixth method closely related to the last one is to require the neutrons to have not only fixed path lengths, but also a limited number of possible directions. Lattice points are set up, and neutrons are required to travel from lattice point to lattice point.

Which of these methods is the most efficient depends on the problem being studied. If the object of the calculation is to obtain a quick answer to a relatively simple problem, direct physical analogy should probably be used by anyone except the most practiced analyst. If the problem is more complicated--and all problems involving space- and energy-dependent neutronics fall in this class--one of the nonanalog methods must be used in order to obtain sufficient accuracy in a reasonable amount of computer time. If the geometry is any more complicated than a two- or three-region cell, the fourth method, the fractional interaction model, is the most efficient.

The determination of the direction of emission from a collision point does not permit the application of such a wide variety of techniques as in the case of space transport. Either the angle of emission is chosen from the known probability distribution function, or the angle of emission is chosen from the isotropic distribution and the neutron weight is multiplied by the actual probability of emission at the selected angle.

There are, however, many alternate ways of tabulating the events in the particle histories. The estimator used depends upon the quantity to be calculated. However, the various scoring methods used can be illustrated for just one quantity, and the methods will apply also to the calculation of other quantities. Suppose that the desired quantities are the probabilities for absorption in hypercubes of phase space. In the direct physical analogy, the number of absorptions in each unit of lethargy and in each unit of volume are recorded and divided by the total number of source neutrons to obtain the absorption probability in each region of phase space. In the modification of the direct physical analogy in which a fraction of the neutron is absorbed at each point, the appropriate absorption estimator is the sum over all collision points of the ratio of the absorption to total cross section times the

neutron weight at each point. The appropriate estimator to be used when the distances between collisions is determined by the scattering cross section only, is the integral of the neutron weight times the absorption cross section over the neutron path length. In this case, the neutron weight is given by

$$\exp\left[-\int_0^s \Sigma_a \, ds\right], \tag{65}$$

where s is the path length.

A scoring method that can be used to reduce the variance in the results is to compute the desired result as the sum of the probable contributions from all scattering points. For example, the absorption probability per source neutron at the point, $\bar{r}_1$, can be computed as

$$\frac{1}{N_s}\sum_{i=0}^{N} w_i \Sigma_s(\bar{r}_i, \bar{\Omega}_i \rightarrow \bar{\Omega}, E_i \rightarrow E) \frac{\exp\left\{-\int_0^s \Sigma_t(\bar{r}_i + s\bar{\Omega}, E)\, ds\right\}}{s^2} \Sigma_a(\bar{r}_1), \tag{66}$$

where

$w_i$ = the neutron weight (initially one, reduced by $\Sigma_s/\Sigma_t$ at each collision),

$$s = |\bar{r}_i - \bar{r}_1|, \tag{67}$$

N = total number of collision points,

$$\bar{\Omega} = \frac{\bar{r}_i - \bar{r}_1}{|\bar{r}_i - \bar{r}_1|}, \tag{68}$$

and

$N_s$ = number of source neutrons.

This method of scoring can sometimes be used to advantage with each of the above-mentioned space-transport models.

## B. Perturbation Methods

### 1. Source Perturbation

If the flux is due to a specified source, $S_1(\bar{X})$, it is possible to choose starting coordinates, $\bar{X}_0$, from a simple function $\bar{S}(\bar{X})$, and obtain

the correct value of the absorption integral, Eq. 35, by correspondingly modifying $g(\bar{X})$. (The notation of Section II-A-2 is used here.) The necessary modification of $g(\bar{X})$ is most easily established by considering the contribution to the sum in Eq. 31 from the points $\bar{X}_{in}$ generated in the nth neutron history. Let $\bar{X}_{on}$ denote the starting coordinates for the nth neutron. The probability of the coordinates $\bar{X}_{on}$ being chosen, when the function $\bar{S}(\bar{X})$ is used, is a factor of $\bar{S}(\bar{X}_{on})/S_1(\bar{X}_{on})$ greater (or less) than the probability of the coordinates $\bar{X}_{on}$ being chosen when the function $S_1(\bar{X})$ is used. Accordingly, the probability of the points $\bar{X}_{in}$ being chosen is increased (or decreased) by the factor $\bar{S}(\bar{X}_{on})/S_1(\bar{X}_{on})$ when the starting coordinates are selected from the distribution $\bar{S}(\bar{X})$ instead of $S_1(\bar{X})$.

Formulating the theory of stochastic evaluation in this way, we immediately observe that we can use one set of neutron trajectories with starting coordinates chosen from a simple distribution, $\bar{S}(\bar{X})$, to obtain results for any number of specified sources, $S_i(\bar{X})$. We consider $S_i(\bar{X})/\bar{S}(\bar{X})$ as a weighting function and refer to this as a multiple weighting technique. The probability that $g(\bar{X}_{in})$ will contribute to the sum in Eq. 31 is multiplied by the same factor. However, to obtain the correct value of the integral, the probable contribution of $g(\bar{X}_{in})$ must remain constant. So, the value of $g(\bar{X}_{in})$ must be divided by $\bar{S}(\bar{X}_{on})/S_1(\bar{X}_{on})$. The value of the integral is therefore given by

$$I = \sum_{i=1}^{N} \frac{g(\bar{X}_i)\, S_1(\bar{X}_{on})}{\bar{S}(\bar{X}_{on})} . \tag{69}$$

As an instructive exercise to develop familiarity with the capabilities of stochastic methods, the technique was applied to obtain the probability of escape from a finite rod, of neutrons incident on the rod with various incident angular distributions. Because of its pedagogic potential, the calculation is described in Appendix A.

### 2. Computation of Temperature Derivatives

The absorption rate in each isotope of a system at a given temperature is easily obtained by the stochastic techniques described in Chapter III. The change in absorption rates as the temperature increases could be obtained by taking the difference between absorption rates computed at two temperatures. However, this method is quite inefficient. An increase in reactor temperature of several hundred degrees will typically produce an increase in absorption rate of about 1%. If the change in absorption rates is desired to two significant digits, the absorption rates must be obtained to four significant digits. Since the statistical error is approximately proportional to the inverse square root of the number of sample points, the time required to obtain four significant digits is a factor of 10,000 greater than the time required to obtain two significant digits.

To compute Doppler reactivity coefficients efficiently, a new method for directly computing the temperature derivative of the absorption rates was derived. The integral to be evaluated is

$$\bar{I} = \frac{\partial}{\partial T} \int \phi(\bar{X})\, \Sigma_a(\bar{X})\, d\bar{X}. \tag{70}$$

Following the usual convention, the temperature dependence of the flux, $\phi$, and the cross sections, $\Sigma_a$ and $\Sigma_t$, is not shown explicitly.

Equation 70 may be written as

$$\bar{I} = \int f(\bar{X})\, \bar{g}(\bar{X})\, d\bar{X}, \tag{71}$$

where

$$\bar{g}(\bar{X}) = \frac{\partial \Sigma_a / \partial T}{\Sigma_t} + \frac{1}{\phi} \frac{\partial \phi}{\partial T} \frac{\Sigma_a}{\Sigma_t} \tag{72}$$

and

$$f(\bar{X}) = \phi(\bar{X})\, \Sigma_t(\bar{X}) \tag{73}$$

as before, so that we can obtain the points $\bar{X}_i$ from the trajectories that are used to compute the absorption rates.

Section C of this chapter discusses the evaluation of the cross sections and their temperature derivatives at each collision point.

A method for evaluating the logarithmic derivative of the flux can be most efficiently and rigorously derived if we remember that the flux in a reactor is the result of the trajectories in phase space of individual neutrons. The flux, $\phi(\bar{X})$, in Eq. 70 is found computationally by following individual trajectories and computing a weight, W, associated with each point of the trajectory. The flux in a unit of volume is, then, proportional to the sum of the weights at all collision points in the volume divided by the macroscopic total cross section.

To determine the temperature derivative of the flux at the ith collision point, we must consider the effect on $W_i$ of a temperature change at all previous collision points. This effect is due to the temperature dependence of the ratio $\Sigma_s/\Sigma_t$ by which W is multiplied at each collision point.

Let $W_i$ denote the weight before the ith collision, $W_{i+1}$ denote the weight after the ith collision, and $R_i$ denote the ratio $\Sigma_s/\Sigma_t$ at the ith collision point. Since the contribution of each neutron to the flux at $\bar{X}_i$ is proportional to $W_i/\Sigma_{ti}$, we can write

$$\frac{1}{\phi}\frac{\partial \phi_i}{\partial T} = \frac{1}{W_i}\frac{\partial W_i}{\partial T} - \frac{1}{\Sigma_{ti}}\frac{\partial \Sigma_{ti}}{\partial T}$$

$$= \frac{1}{W_{i-1}R_{i-1}}\frac{\partial (W_{i-1}R_{i-1})}{\partial T} - \frac{1}{\Sigma_{ti}}\frac{\partial \Sigma_{ti}}{\partial T}$$

$$= \frac{1}{R_{i-1}}\frac{\partial R_{i-1}}{\partial T} + \frac{1}{W_{i-1}}\frac{\partial W_{i-1}}{\partial T} - \frac{1}{\Sigma_{ti}}\frac{\partial \Sigma_{ti}}{\partial T}$$

$$= \frac{1}{R_{i-1}}\frac{\partial R_{i-1}}{\partial T} + \frac{1}{R_{i-2}}\frac{\partial R_{i-2}}{\partial T} + \cdots + \frac{1}{R_1}\frac{\partial R_1}{\partial T} + \frac{1}{W_0}\frac{\partial W_0}{\partial T} - \frac{1}{\Sigma_{ti}}\frac{\partial \Sigma_{ti}}{\partial T}$$

$$= \sum_{p=1}^{i-1}\left[\frac{\Sigma_t}{\Sigma_s}\frac{\partial}{\partial T}\left(\frac{\Sigma_s}{\Sigma_t}\right)\right]_p - \frac{1}{\Sigma_{ti}}\frac{\partial \Sigma_{ti}}{\partial T}$$

$$= \sum_{p=1}^{i-1}\left[\frac{1}{\Sigma_s(\bar{X}_p)}\frac{\partial \Sigma_s(\bar{X}_p)}{\partial T} - \frac{1}{\Sigma_t(\bar{X}_p)}\frac{\partial \Sigma_t(\bar{X}_p)}{\partial T}\right] - \frac{1}{\Sigma_{ti}}\frac{\partial \Sigma_{ti}}{\partial T}. \qquad (74)$$

The cross sections and their derivatives are evaluated and the required sums accumulated as each neutron history is traced.

### 3. Variation in Fuel-element Diameter

As part of this research to study the effect of heterogeneity on the Doppler coefficient in fast reactors, it was desired to compare the Doppler coefficient in two reactor systems having identical fuel and moderator volume fractions, but different-sized fuel elements. Computing the Doppler coefficient in each system and obtaining the difference by subtraction are complicated by statistical errors. To avoid this difficulty, a method of computing the Doppler coefficient for two such systems using one set of neutron histories was developed based on the fact that two geometrically similar transport problems have identical solutions if each product of distance times cross section in one system is identical to the corresponding product in the other system.

Dresner has shown that this equivalence theorem is true for various approximate models. That it is true in any system to which the transport equation applies, can be shown by comparing the integral transport

equations for equivalent systems. The space- and energy-dependent flux in one system is given by the equation

$$\phi_1(\bar{r}, E) = \frac{1}{4\pi} \int \int_{V_1} \int |\bar{r} - \bar{r}'|^{-2} \exp[-|\bar{r} - \bar{r}'| \Sigma_t(E)]$$

$$\cdot \left\{ \int \phi_1(\bar{r}', E') \, C(E') \, \Sigma_t(E') \, f(E' \rightarrow E) \, dE' + 4\pi S_1(\bar{r}', E) \right\} dV', \quad (75)$$

and the equation for an equivalent system K times as large (with cross section $\Sigma_t(E)/K$) is

$$\phi_2(\bar{X}, E) = \frac{1}{4\pi} \int \int_{V_2} \int |\bar{X} - \bar{X}'|^{-2} \exp(-|\bar{X} - \bar{X}'| \Sigma_t/K)$$

$$\cdot \left\{ \int \phi_2(\bar{X}', E') \, C(E') \, [\Sigma_t(E')/K] \, f(E' \rightarrow E) \, dE' + 4\pi S_2(\bar{X}', E) \right\} dV', \quad (76)$$

where

$\phi_i$ = the neutron flux in system i,

$V_i$ = the volume of system i,

$\Sigma_t$ = the total macroscopic cross section of system one,

$C$ = the expected number of neutrons emitted per collision,

$f(E' \rightarrow E)$ = the probability that a neutron emitted from a collision of a neutron of energy $E'$, will have the energy $E$,

and

$S_i$ = the neutron source density in system i.

With the substitutions

$$\bar{X} = K\bar{r} \text{ and } \bar{X}' = K\bar{r}', \quad (77)$$

Eq. 76 becomes

$$\phi_2(K\bar{r}, E) = \frac{1}{4\pi}\int \int_{V_1} \int |K\bar{r} - K\bar{r}'|^{-2} \exp[-|K\bar{r} - K\bar{r}'|\Sigma_t(E)/K]$$

$$\cdot \left\{ \int \phi_2(K\bar{r}', E') \, C(E') \, [\Sigma_t(E')/K] \, f(E' \rightarrow E) \, dE' + 4\pi S_2(K\bar{r}', E) \right\} K^3 dV'. \tag{78}$$

When Eq. 78 is simplified by cancelling $K^3/K^3$, it becomes

$$\phi_2(K\bar{r}, E) = \frac{1}{4\pi}\int \int_{V_1} \int |\bar{r} - \bar{r}'|^{-2} \exp[-|\bar{r} - \bar{r}'|\Sigma_t]$$

$$\cdot \{\phi_2(K\bar{r}', E') \, C(E') \, \Sigma_t(E') \, f(E' \rightarrow E) \, dE' + 4\pi S_2(K\bar{r}', E) \, K\} \, dV'. \tag{79}$$

Comparing Eqs. 79 and 75, we see that if we take

$$S_2(K\bar{r}, E) = S_1(\bar{r}, E)/K, \tag{80}$$

then $\phi_2(K\bar{r}, E)$ must be identically equal to $\phi_1(\bar{r}, E)$.

For the systems to be equivalent, the external source in the second system must be $K^{-1}$ times the source in the first system. Also, K must be independent of energy but may be a function of space.

This equivalence makes it possible to study the effect of heterogeneity in systems composed of identical materials but different dimensions, by studying the corresponding systems having identical dimensions but different macroscopic cross sections.

The Doppler coefficient for two such systems may be computed using one set of neutron histories. The histories are generated for one of the systems using the fractional interaction model, discussed below, and the Doppler coefficient for this system is obtained using an absorption-derivative (with respect to temperature) estimator. The Doppler coefficient for the second system is obtained at the same time in the same way, except that the neutron weight for this system is multiplied at each collision by the factor

$$F = \frac{\Sigma_{t2}}{\Sigma_{t1}} \exp[(\Sigma_{t1} - \Sigma_{t2}) \, x], \tag{81}$$

where

$\Sigma_{t1}$ = the macroscopic total cross section in the first system,

$\Sigma_{t2}$ = the macroscopic total cross section in the second system,

and

x = the distance between collisions.

Since the free path lengths are selected from the probability density function

$$P_1(x) = \Sigma_{t1} \exp(-\Sigma_{t1}x), \tag{82}$$

the factor, F, is the importance function required to obtain the correct answer in the second system in which the probability density function for free path lengths is

$$P_2(x) = \Sigma_{t2} \exp(-\Sigma_{t2}x); \tag{83}$$

i.e., F is the ratio of $P_2(x)$ to $P_1(x)$. That F is the correct importance function can be established by the following argument. If $\Sigma_{t2}$ is less than $\Sigma_{t1}$, then choosing the path length, x, from the distribution

$$P_1(x) = \Sigma_{t1} \exp(-\Sigma_{t1}x) \tag{84}$$

will result in too many path lengths shorter than $1/\Sigma_{t2}$. To compensate for this, the weights of neutrons with short path lengths are decreased by the factor F. The effective (weighted) distribution of path length is

$$P_1(x)\, F(x) = [\Sigma_{t1} \exp(-\Sigma_{t1}x)]\left\{\frac{\Sigma_{t2}}{\Sigma_{t1}} \exp[(\Sigma_{t1} - \Sigma_{t2})\, x]\right\}$$

$$= \Sigma_{t2} \exp(-\Sigma_{t2}x), \tag{85}$$

which is the correct distribution of path lengths in system 2.

## C. Special Techniques

### 1. An Absolutely Random Number Generator

Basic to all stochastic techniques is a method of generating random numbers satisfying some known probability distribution. No satisfactory method for generating truly random numbers was known previously,

so it became customary to use numbers from a pseudo-random chain generated by the multiplicative or mixed congruential method. As part of this research, a method of obtaining random numbers by sampling arbitrary memory locations in a digital computer was developed. Previous attempts to obtain random numbers by sampling memory locations have failed because of inevitable bias in the results. A new technique for eliminating this bias was developed and used as the basis for an absolutely random number generator. In its simplest form the technique is as follows:

Identical bit positions of successive memory locations are sampled. If the two sampled bits are (0, 0) or (1, 1), the result is discarded and another sample is taken. If the result is (0, 1) or (1, 0) then 0 or 1, respectively, is taken to be the first bit of our random number. The remaining bits are selected similarly. This procedure completely eliminates any bias due to an excess of "0" or "1" bits in the memory, since the probability of obtaining (0, 1) is exactly equal to the probability of obtaining (1, 0). Serial and moments tests of this procedure have verified the randomness of numbers selected in this way. However, the time required to obtain a random number by this procedure exceeds the time required to obtain a pseudo-random number by the multiplicative congruential technique.

## 2. The Fractional Interaction Model

The standard method of tracking neutrons in heterogeneous systems requires the calculation of the optical distances from the point of each collision to each of the region boundary points through which the neutron passes on its flight to the next collision. This is a very time-consuming process, and the possibility of avoiding it merits serious attention because of the potential savings in computing time.

A rigorous mathematical theory for a technique that eliminates the calculation of intermediate optical distances is given here. Calculations performed on a CDC-3600 computer using this technique indicate that the required computing time to obtain a given accuracy is reduced by a factor of two or three, compared to the time required for standard tracking techniques.

Following a suggestion implicit in Chilton's work[22] on thick shields, the steady-state transport equation can be written in the form

$$\bar{\Omega} \cdot \nabla\phi(\bar{r}, E, \bar{\Omega}) + C(\bar{r}, E)\,\phi(\bar{r}, E, \bar{\Omega}) = \int\int P(E', \bar{\Omega}' \to E, \bar{\Omega})\,\Sigma_s(\bar{r}, E')\,\phi(\bar{r}, E', \bar{\Omega}')\,dE d\bar{\Omega}'$$

$$+ [C(\bar{r}, E) - \Sigma_t(\bar{r}, E)]\,\phi(\bar{r}, E, \bar{\Omega}) + s(\bar{r}, E, \bar{\Omega}), \qquad (86)$$

where

$\Sigma_t$ = the total macroscopic cross section of the medium,

$\Sigma_s$ = the macroscopic scattering cross section of the medium,

and

$C$ = a fictitious cross section such that $C \geq \Sigma_t$.

This suggests that the flux can be considered to be the average density of trajectories generated by particles that migrate according to the following rules. The particles travel with constant velocity between collisions and may change velocity but not position in collisions. The distance between collisions is given by the probability-density function,

$$f(s) = C(\bar{r}, E) \exp\left[-\int_0^s C(\bar{r}, E)\, ds\right]. \tag{87}$$

When a collision occurs at phase point $(\bar{r}, E, \bar{\Omega})$, there is a probability given by

$$\frac{\Sigma_s(\bar{r}, E, \bar{\Omega})\, P(E, \bar{\Omega} \rightarrow E', \bar{\Omega}')}{C(\bar{r}, E)} \tag{88}$$

that the neutron will be transferred to phase point $(r, \bar{E}', \bar{\Omega}')$. Also there is an independent probability that a neutron will be emitted at $(\bar{r}, E, \bar{\Omega})$ given by

$$\frac{C(\bar{r}, E) - \Sigma_t(\bar{r}, E)}{C(\bar{r}, E)}. \tag{89}$$

We could use this model to simplify the solution of the Boltzmann equation by choosing $C(\bar{r}, E)$ independent of $\bar{r}$. However, this model introduces the complication of branching of trajectories.

We can eliminate branching of trajectories by an arbitrary change in the model. The form of the modification is suggested by the arguments of Steen[15,85] and Woodcock *et al.*[100] concerning the use of a fictitious scattering process called "delta scattering" by Steen. We will show rigorously that this modified model correctly represents neutron transport.

We make the probability of emission of a new neutron contingent on the result of the collision of the original neutron. If the original neutron is scattered or absorbed, i.e., if a random number, $\rho$, satisfies $\rho < \Sigma_t(\bar{r}, E)/C(\bar{r}, E)$, the probability of emission of a new neutron by the fictitious source is taken as zero; otherwise it is one.

Hence the possibility of a scattered neutron appearing at $(\bar{r}, E', \bar{\Omega}')$ simultaneously with a new neutron at $(\bar{r}, E, \bar{\Omega})$ is eliminated, and we can consider any new neutron emitted by the source $[C(\bar{r}, E) - \Sigma_t(\bar{r}, E)] \cdot \phi(\bar{r}, E, \bar{\Omega})$, to be the reincarnation of the original particle. So at each collision, there are three mutually exclusive possibilities. The neutron is absorbed, scattered, or not changed at all. The probability of interaction is given by $\Sigma_t(\bar{r}, E)/C(\bar{r}, E)$, and the probability of no interaction is given by $[C(\bar{r}, E) - \Sigma_t(\bar{r}, E)]/C(\bar{r}, E)$. This corresponds to Woodcock's model.

The validity of this model, which we will call the fractional interaction model, can be shown rigorously by comparing the distribution of free path lengths between true collisions generated by this model with the known physically correct distribution.

As a first step, we show that the mean free path and the mean-square path length generated by the fractional interaction model are identical to the physically correct mean free path and mean-square path lengths.

In the fractional interaction model, the distance traveled is found by first computing $x_1$ from the integral equation,

$$\int_0^{x_1} Ce^{-Cx}\, dx = \rho_1; \tag{90}$$

i.e.,

$$x_1 = -\frac{1}{C} \ln \rho_1, \tag{91}$$

where C is the fictitious cross section and $\rho_1$ is a random number from the uniform distribution on [0, 1].

The probability, $P_1$, that this is a true interaction point and $x_1$ is the path length, is $\Sigma_t/C$.

Similarly, there is a probability,

$$P_2 = \left(\frac{C - \Sigma_t}{C}\right)\left(\frac{\Sigma_t}{C}\right), \tag{92}$$

that the total distance traveled before a true collision will be $x_1 + x_2$, where

$$x_i = -\frac{1}{C} \ln \rho_i. \tag{93}$$

In general, there is a probability,

$$P_n = \left(\frac{C - \Sigma_t}{C}\right)^{n-1}\left(\frac{\Sigma_t}{C}\right), \tag{94}$$

that the total distance traveled will be

$$d_n \equiv \sum_{i=1}^{n} x_i. \tag{95}$$

The expected value for the free path length is, therefore,

$$\langle d \rangle = \left\langle \sum_{n=1}^{\infty} P_n d_n \Big/ \sum_{n=1}^{\infty} P_n \right\rangle \tag{96}$$

$$= \frac{\sum_{n=1}^{\infty} P_n \langle d_n \rangle}{\sum_{n=1}^{\infty} P_n}. \tag{97}$$

The sum in the denominator is

$$\sum_{n=1}^{\infty} P_n = \sum_{n=1}^{\infty} \frac{\Sigma_t}{C}\left(1 - \frac{\Sigma_t}{C}\right)^{n-1} \tag{98}$$

$$= \frac{\Sigma_t}{C} \sum_{n=0}^{\infty} \left(1 - \frac{\Sigma_t}{C}\right)^{n} \tag{99}$$

$$= \frac{\Sigma_t}{C}\left[1 - \left(1 - \frac{\Sigma_t}{C}\right)\right]^{-1} \tag{100}$$

$$= 1.$$

To evaluate the numerator, we note that the expected value of a sum is equal to the sum of expected values; i.e.,

$$\left\langle \sum_{i=1}^{n} -\frac{1}{C} \ln \rho_i \right\rangle = \sum_{i=1}^{n} \left\langle -\frac{1}{C} \ln \rho_i \right\rangle. \tag{101}$$

The expected value of each term in the sum on the right is

$$\left\langle -\frac{1}{C} \ln \rho_i \right\rangle = \int_0^1 -\frac{1}{C} \ln \rho \, d\rho = \frac{1}{C}. \tag{102}$$

Therefore the expected value of the sum on the left is simply n/C. Also, we will need to use the identity

$$\sum_{n=0}^{\infty} n x^{n-1} = \frac{1}{(1-x)^2}, \tag{103}$$

which results from differentiating the familiar identity

$$\sum_{n=0}^{\infty} x^n = \frac{1}{1-x}.$$

Using these two results, we find that the numerator is

$$\sum_{n=1}^{\infty} \frac{\Sigma_t (C - \Sigma_t)^{n-1}}{C^n} \left\langle \sum_{i=1}^{n} -\frac{1}{C} \ln \rho_i \right\rangle$$

$$= \frac{\Sigma_t}{C^2} \sum^{\infty} \left(\frac{C - \Sigma_t}{C}\right)^{n-1} \cdot n$$

$$= \frac{\Sigma_t}{C^2} \, 1 - \left(\frac{C - \Sigma_t}{C}\right)^{-2} = \frac{1}{\Sigma_t}. \tag{104}$$

Therefore, the expected value of the free path length in the fractional interaction model is

$$\langle d \rangle = \frac{1}{\Sigma_t}, \tag{105}$$

which is physically correct.

Similarly, the mean-square path length (i.e., the second moment of the path-length distribution) produced by the model is

$$\langle d^2 \rangle = \left\langle \sum_{n=1}^{\infty} P_n d_n^2 \Big/ \sum_{n=1}^{\infty} P_n \right\rangle$$

$$= \frac{\sum_{n=1}^{\infty} P_n \langle d_n^2 \rangle}{\sum_{n=1}^{\infty} P_n}$$

$$= \sum_{n=1}^{\infty} P_n \int_0^1 \cdots \int_0^1 \frac{1}{C^2} \left( \sum_{i=1}^{n} - \ln \rho_i \right)^2 d\rho_1 \cdots d\rho_n$$

$$= \sum_{n=1}^{\infty} \frac{\Sigma_t}{C} \left( 1 - \frac{\Sigma_t}{C} \right)^{n+1} \left[ n + \binom{n}{2} \right] \frac{2}{C^2}$$

$$= \frac{\Sigma_t}{C^3} \sum_{n=1}^{\infty} \left( 1 - \frac{\Sigma_t}{C} \right)^{n-1} (n^2 + n)$$

$$= \frac{2\Sigma_t}{C^3} \left( 1 - 1 + \frac{\Sigma_t}{C} \right)^{-3}$$

$$= \frac{2}{\Sigma_t^2}. \tag{106}$$

Here we have used the identities

$$\int_0^1 \cdots \int_0^1 \left( \sum_{i=1}^{n} -\ln \rho_i \right)^2 d\rho_1 \cdots d\rho_n = n^2 + n, \tag{107}$$

and

$$\sum_{n=1}^{\infty} (n^2 + n)\, x^{n-1} = 2(1 - x)^{-3}. \tag{108}$$

The first can be derived by noting that the integrand consists of $n + \binom{n}{2}$ terms, and the integral of each term is 2. The second is found by differentiating the familiar identity

$$\sum_{n=0}^{\infty} (n+1)\, x^n = (1-x)^{-2}. \tag{109}$$

The second moment of the physical distribution of mean free paths is known to be

$$\int_0^{\infty} x^2 \Sigma_t e^{-\Sigma_t x}\, dx = \frac{2}{\Sigma_t^2}, \tag{110}$$

which is the same as the second moment of the distribution generated by the fractional interaction model. So the first and second moments of the model distribution are identical to the first and second moments of the physical distribution.

In general, the mth moment of the path-length distribution produced by the model is, for m = 1, 2, 3, ..., ∞,

$$\begin{aligned}
\langle d^m \rangle &= \left\langle \sum_{n=1}^{\infty} P_n d_n^m \Big/ \sum_{n=1}^{\infty} P_n \right\rangle \\
&= \sum_{n=1}^{\infty} P_n \langle d_n^m \rangle \Big/ \sum_{n=1}^{\infty} P_n \\
&= \sum_{n=1}^{\infty} P_n \int_0^1 \cdots \int_0^1 \frac{1}{C^m} \left( \sum_{i=1}^{n} -\ln \rho_i \right)^m d\rho_1 \cdots d\rho_n \\
&= \sum_{n=1}^{\infty} \frac{\Sigma_t}{C} \left(1 - \frac{\Sigma_t}{C}\right)^{n-1} \frac{(n+m-1)!}{(n-1)!} \frac{1}{C^m} \\
&= (m!)\, \frac{\Sigma_t}{C^{m+1}} \left(1 - 1 + \frac{\Sigma_t}{C}\right)^{-(m+1)}
\end{aligned} \tag{111}$$

or

$$\langle d^m \rangle = \frac{m!}{\Sigma_t^m}. \tag{112}$$

We have used the identities

$$\int_0^1 \cdots \int_0^1 \left( \sum_{i=1}^{n} -\ln \rho_i \right)^m d\rho_1 \cdots d\rho_n = \frac{(n+m-1)!}{(n-1)!} \tag{113}$$

and

$$\sum_{n=1}^{\infty} \frac{(n+m-1)!}{(n+1)} x^{n-1} = m!(1-x)^{-(m+1)} \tag{114}$$

To prove the first of these identities, we will need the following identity:

$$\sum_{K=0}^{m} \frac{(N-2+K)!m!}{K!(N-2)!} = \frac{(N+m-1)!}{(N-1)!}, \tag{115}$$

which is equivalent to

$$\sum_{K=0}^{m} \frac{(N-2+K)!}{K!} = \frac{(N+m-1)!}{m!(N-1)} \tag{116}$$

The validity of this identity can be shown by mathematical induction; i.e.,

1) It is true for m = 0, by direct substitution.

2) If it is true for m = M - 1, i.e.,

$$\sum_{K=0}^{M-1} \frac{(N-2+K)!}{K!} = \frac{(N+M-2)!}{(M-1)!(N-1)}, \tag{117}$$

then

$$\begin{aligned} \sum_{K=0}^{M} \frac{(N-2+K)!}{K!} &= \frac{(N+M-2)!}{(M-1)!(N-1)} + \frac{(N-2+M)!}{M!} \\ &= \frac{M(N+M-2)! + (N-1)(N+M-2)}{M!(N-1)} \\ &= \frac{(N+M-1)!}{M!(N-1)} \end{aligned} \tag{118}$$

and it is true for m = M. Therefore, it is true for all m for any value of n.

Using this result, we can prove the first identity by mathematical induction. It is true for n = 1. (See Handbook of Chemistry and Physics, 45th Edition, definite integral No. 433.) Suppose it is true for n = N - 1. Then,

$$\int_0^1 \cdots \int_0^1 \left( \sum_{i=1}^{N} -\ln \rho_i \right)^m d\rho_1 \cdots d\rho_N$$

$$= \int_0^1 \cdots \int_0^1 \left( \sum_{i=1}^{N-1} -\ln \rho_i - \ln \rho_N \right)^m d\rho_1 \cdots d\rho_N$$

$$= \int_0^1 \cdots \int_0^1 \sum_{K=0}^{m} \binom{m}{K} \left( \sum_{i=1}^{N-1} -\ln \rho_i \right)^K (-\ln \rho_N)^{m-K} \, d\rho_1 \cdots d\rho_N$$

$$= \sum_{K=0}^{m} \binom{m}{K} \int_0^1 (-\ln \rho_N)^{m-K} \, d\rho_N \int_0^1 \cdots \int_0^1 \left( \sum_{i=1}^{N-1} -\ln \rho_i \right)^K d\rho_1 \cdots d\rho_{N-1}$$

$$= \sum_{K=0}^{m} \frac{m!}{K!(m-K)!} \frac{(m-K)!}{1} \frac{(N+K-2)!}{(N-2)!}$$

$$= \frac{(N+m-1)!}{(N+1)!}, \tag{119}$$

and it is true for n = N. Then it is true for all n for any value of m.

The second identity can also be proven by mathematical induction. It is true for m = 1, by direct substitution. If it is true for m = M - 1, i.e.,

$$\sum_{n=1}^{\infty} \frac{(n+M-2)!}{(n-1)!} x^{n-1} = (M-1)!(1-x)^{-M}, \tag{120}$$

then differentiating with respect to x gives

$$\sum_{n=1}^{\infty} \frac{(n+M-2)!}{(n-1)!}\,(n-1)\,x^{n-2} = M!(1-x)^{-(M+1)}$$

$$\sum_{n=2}^{\infty} \frac{(n+M-2)!}{(n-2)!}\,x^{n-2} = M!(1-x)^{-(M+1)}$$

$$\sum_{n=1}^{\infty} \frac{(n+M-1)!}{(n-1)!}\,x^{n-1} = M!(1-x)^{-(M+1)}, \tag{121}$$

and it is true for m = M. Therefore it is true for all M.

The mth moment of the physical distribution is

$$\int_0^{\infty} x^m \Sigma_t e^{-\Sigma_t x}\,dx = \frac{m!}{\Sigma_t^m}. \tag{122}$$

Thus all the moments of the fractional interaction model distribution are identical to the moments of the physical distribution. However, this is a necessary but not sufficient condition for the identity of the two distributions.

This is a variation of the Stieltjes moment problem,[94] which is to find a nondecreasing function $\phi(x)$ taking on infinitely many values in the interval $(0, \infty)$, such that

$$C_n = \int_0^{\infty} x^n\,d\phi(x) \qquad n = 0, 1, 2, \ldots, \infty, \tag{123}$$

given $C_0, C_1, C_2, \ldots$ . Carleman's Theorem[16] states that if a solution to a Stieltjes moment problem exists, a sufficient condition for the uniqueness of the solution is divergence of the series

$$\sum_{n=0}^{\infty} \left(\frac{1}{C_n}\right)^{\frac{1}{2n}}. \tag{124}$$

Since the series

$$\sum_{m=0}^{\infty} \left(\frac{\Sigma_t^m}{m!}\right)^{\frac{1}{2m}} \tag{125}$$

is divergent, our Stieltjes problem has a unique solution.

The divergence of the series is shown by the ratio test. Expanding the $(m+1)$st term, as follows,

$$\left(\frac{\Sigma_t^{m+1}}{(m+1)!}\right)^{\frac{1}{2(m+1)}} = \left(\frac{\Sigma_t}{m+1}\right)^{\frac{1}{2(m+1)}} \left(\frac{\Sigma_t^m}{m!}\right)^{\frac{1}{2(m+1)}}$$

$$= \left(\frac{\Sigma_t}{m+1}\right)^{\frac{1}{2(m+1)}} \left(\frac{\Sigma_t^m}{m!}\right)^{\frac{-1}{2m(m+1)}} \left(\frac{\Sigma_t^m}{m!}\right)^{\frac{1}{2m}} \tag{126}$$

shows that the ratio of the $(m+1)$st to the nth term is

$$\left(\frac{\Sigma_t}{m+1}\right)^{\frac{1}{2(m+1)}} \left(\frac{\Sigma_t^m}{m!}\right)^{\frac{-1}{2m(m+1)}}, \tag{127}$$

which can be written as

$$(\Sigma_t)^{\frac{1}{2(m+1)}} (\Sigma_t)^{\frac{1}{2m(m+1)}} \left(\frac{1}{m+1}\right)^{\frac{1}{2(m+1)}} \left(\frac{1}{m!}\right)^{\frac{-1}{2m(m+1)}} \tag{128}$$

The limits of the first and second factors as $m \to \infty$ are equal to 1. To find the limit of the third factor, we note that

$$\lim_{n\to\infty} \ln \left(\frac{1}{m+1}\right)^{\frac{1}{2(m+1)}} = \lim_{m\to\infty} \left(\frac{1}{2(m+1)} \ln \frac{1}{m+1}\right) = 0. \tag{129}$$

Therefore,

$$\lim_{m\to\infty} \left(\frac{1}{m+1}\right)^{\frac{1}{m+1}} = 1. \tag{130}$$

Similarly, the limit of the fourth term as $m \to \infty$ is 1. Combining these results, the ratio of the $(n+1)$st to the nth terms of the series is 1. So the series is divergent by the ratio test, and the sufficient condition for the uniqueness of the solution to our Stieltjes problem is established.

In conclusion, all the moments of the path-length distribution produced by the fractional interaction model are identical to the corresponding moments of the physically correct distribution, and there is only one distribution with this set of moments.

Therefore, the distribution of free path lengths produced by the fractional interaction model is identical to the physically correct distribution.

We have shown that the fractional interaction model produces the correct distribution of neutron path lengths in a homogeneous medium. This proof can be extended to heterogeneous media by considering the distribution of path lengths for those neutrons that cross a boundary before suffering a collision. These neutrons should produce a path-length distribution in the second media corresponding to the probability density function

$$f(x) = \Sigma_2 e^{-\Sigma_2 x}, \tag{131}$$

where $\Sigma_2$ is the total cross section in the second media. Using the fractional interaction model, the distances to the first collisions of these neutrons are distributed according to the probability density function,

$$P(x) = Ce^{-(x+S_1)C} e^{S_1 C} = Ce^{-Cx}, \tag{132}$$

where

$S_1$ = the distance traveled in the first media,

and

$e^{S_1 C}$ = the normalization factor required to make $\int P(x)\,dx = 1$.

The first collision is accepted as a true collision if $\rho < \Sigma_2/C$. Otherwise, the neutron continues in its original direction a distance chosen from $P(x)$. This method has been shown to produce the path-length distribution

$$f(x) = \Sigma_2 e^{-\Sigma_2 x}. \tag{133}$$

Therefore, the fractional interaction model produces the correct path-length distribution in the second media for those particles that cross the boundary.

3. The Source Distribution

If the neutron trajectories are traced from a sufficiently high energy, the form of the source is not important. The flux as a function of energy in the energy range where the Doppler effect occurs will be determined correctly as the neutrons are scattered through the higher-energy region. However, determining the neutron source in this way requires considerable tracking of neutrons outside the energy region of interest and significantly increases the required computing time. An alternative procedure is to compute the neutron source for the Doppler region using the assumption that the flux is asymptotic above the Doppler region. In some cases this may be a reasonable assumption, but in many cases, particularly in reactors without significant moderator, it is not.

A reasonable description of the energy dependence of the neutron source for the Doppler region can be given for a particular reactor by specifying a value for the exponent, a, in the expression

$$\phi \propto 1/E^a. \tag{134}$$

If the flux as a function of energy is specified in this way for the energy region between the maximum energy of interest, $E_1$, and $E_1/\alpha$, where $\alpha$ is the maximum fractional change in energy that a neutron can suffer in an elastic collision with the lightest isotope present, then the neutron source in the energy region below $E_{max}$ due to scattering collisions with the nth isotope is

$$S_n = \int_{E_1}^{E/\alpha_n} \Sigma_s \frac{1}{E^a} \frac{1}{(1-\alpha_n)\,E}\, dE. \tag{135}$$

Performing the integration gives

$$S_n = \Sigma_s \frac{1}{(1-\alpha_n)\,a}\left[\left(\frac{1}{E_1}\right)^a - \left(\frac{\alpha_n}{E}\right)^a\right]. \tag{136}$$

The total source due to each nuclide is proportional to

$$P_n = \int_{\alpha_n E_1}^{E_1} S_n(E)\, dE. \tag{137}$$

Performing the integration gives

$$P_n = \Sigma_s E_l^{1-a}\left[\frac{a}{1-\alpha_n} + \frac{\alpha_n}{1-a} - \frac{(\alpha_n)^a}{(1-a)\,a}\right] \quad \text{for } a \neq 1; \tag{138}$$

$$P_n = \xi\Sigma_s \quad \text{for } a = 1. \tag{139}$$

The probability that a neutron scatters into the energy range of interest due to a collision with the nth isotope in the jth region is

$$\frac{P_{n,j}V_j}{\sum_{j=1}^{J}\sum_{n=1}^{N_j} P_{n,j}V_j} \tag{140}$$

where

$V_j$ = volume of the jth region,

$N_j$ = the number of isotopes in the jth region,

$J$ = the number of spacial regions,

and

$P_{n,j}$ = total source due to the nth nuclide in the jth region.

The spacial region in which each neutron is scattered from above $E_l$ to below $E_l$ can be determined by solving for j' in the equation

$$\frac{\sum_{j=1}^{j'-1}\sum_{n=1}^{N_j} P_{n,j}V_j}{S} < \rho < \frac{\sum_{j=1}^{j'}\sum_{n=1}^{N_j} P_{n,j}V_j}{S}, \tag{141}$$

where $\rho$ is a random number and

$$S = \sum_{j=1}^{J}\sum_{n=1}^{N_j} P_{n,j}V_j. \tag{142}$$

This is easily done since j takes on only small integer values. Also the equation

$$\frac{\sum_{n=1}^{n'-1} P_{n,j'}}{P_{j'}} < \rho < \frac{\sum_{n=1}^{n'} P_{n,j'}}{P_{j'}}, \tag{143}$$

where

$$P_{j'} = \sum_{n=i}^{N_{j'}} P_{n,j'} \tag{144}$$

is easily solved for n' to determine the scattering nuclide.

However, solving the appropriate integral equation for the initial energy below $E_1$ would be more difficult. This can be avoided by choosing E from the uniform normalized distribution

$$S'_n(E) = \frac{1}{E_1(1-\alpha_n)} \tag{145}$$

and setting the starting neutron weight equal to

$$\frac{S_n(E)}{S'_n(E)}. \tag{146}$$

(See Section B of this chapter for a discussion of the correct procedure for selecting from an arbitrary source.)

4. Evaluation of Cross Sections

To accurately treat the energy dependence of the collision density, and to avoid the uncertainties introduced in earlier Monte Carlo codes by interpolation of a necessarily limited table of cross sections vs energy, the cross sections of all materials are computed from the resonance parameters at each energy of each neutron. The Doppler-broadened cross sections are given by Eqs. 22 and 23. Differentiation of these equations and use of the relations[89]

$$\frac{\partial \psi}{\partial T} = \frac{1}{2T}\left[\left(\frac{x^2-1}{2\theta} - 1\right)\psi - \frac{x}{\theta}\chi + \frac{1}{2\theta}\right] \tag{147}$$

and

$$\frac{\partial \chi}{\partial T} = \frac{1}{2T}\left[\left(\frac{x^2-1}{2\theta}\right)\chi + \frac{x}{\theta}\psi - \frac{x}{2\theta}\right] \tag{148}$$

yields equations for $\partial\sigma_a/\partial T$ and $\partial\sigma_s/\partial T$ in terms of the Doppler-line-shape functions, $\psi(x,\theta)$ and $\chi(x,\theta)$. One of the algorithms of O'Shea and Thacher[72] is used to evaluate these functions at each neutron energy for each of a given number of resonance levels above and below the neutron energy, using the resonance parameters specified as input.

Resonance parameters for the lowest-energy resonances of most isotopes have been obtained from experimental measurements. For example, the 217 resonances of $U^{238}$ between 0 and 4.0 keV have been resolved.[38] The average value and distribution of level widths and spacing of the resolved resonances may be determined and used to select a set of resonance parameters for the unresolved region. The distribution of reduced neutron widths, fission widths, and capture widths have been found to approximate Chi-squared distributions with 1, 2, and $\infty$ degrees of freedom, respectively.[73] For example, the distribution of reduced neutron widths $\Gamma_n^0$ is given by the probability distribution

$$P(x) = \frac{\eta(\eta x)^{\eta-1}e^{-\eta x}}{\Gamma(\eta)}, \tag{149}$$

with $\eta = 1/2$, where

$$x = \frac{\Gamma_n^0}{\langle\Gamma_n^0\rangle}$$

$\Gamma(\eta)$ is the gamma function,

and

$\eta$ = one-half the number of degrees of freedom.

The level spacings follow the Wigner distribution,

$$P(y) = \frac{\pi}{2} y e^{-\frac{\pi}{4}y^2}, \tag{150}$$

where

$$y = \frac{D}{\langle\bar{D}\rangle}.$$

The level spacings, fission widths, and capture widths are determined from the explicit formulas

$$D = \langle D \rangle \sqrt{-\ln \rho}\,(2/\sqrt{\pi}), \tag{151}$$

$$\Gamma_f = -\langle \Gamma_f \rangle \ln \rho, \tag{152}$$

and

$$\Gamma_\gamma = \langle \Gamma_\gamma \rangle, \tag{153}$$

where $\rho$ denotes a different random number in each formula each time it is used. Resonance parameters are determined in this way, starting from the highest resolved resonance and continuing until resonance parameters have been determined for the entire energy region of interest, or until the limit of core storage is reached. In the latter case, the cross sections in the energy region above the highest resonance are computed by choosing an energy in the region covered by the resonance parameters, and computing the cross sections that would result if the surrounding resonances were instead located around the higher energy of interest. The variation of $\Gamma_n$ with energy is taken into account by multiplying the $\Gamma_n$ of the lower resonance by the square root of the ratio of the higher to the lower energy.

# CHAPTER III

# IMPLEMENTATION OF THE THEORY

## A. Logical Sequence and Description of the Calculation

The theory formulated in Chapter II was combined with other carefully selected numerical and stochastic techniques in the new Monte Carlo code, AMC (Argonne Monte Carlo). The logical sequence of the calculation incorporating these techniques is described here.

### 1. Logical Sequence

After the initial coordinates of each neutron in phase space are determined, as described in Chapter II, the absorption, scattering, and fission cross sections for a neutron of the selected initial energy are computed for all regions. The distance the neutron travels before its first collision is then determined using the fractional interaction model, and simple trigonometry is used to find the coordinates of the first collision. The position of the neutron is specified by the indices of the cell it is in and its rectangular Cartesian coordinates in the cell. A series of simple tests determines the cell indices and the region of the cell containing the neutron. The probabilities of absorption and fission at this collision point, $\Sigma_a^n/\Sigma_t$ and $\Sigma_F^n/\Sigma_t$, for each nuclide, n, in the region are multiplied by the neutron weight and tabulated as this neutron's contribution to the absorption and fission probabilities in the hypercube of phase space containing this collision point. Correspondingly, the neutron weight is reduced by the factor $\Sigma_s/\Sigma_t$. The neutron leaves the collision in a direction determined by three random numbers. The exit energy of the neutron is easily calculated. Assuming that energy and momentum are conserved in the center-of-mass system, the energy of the scattered neutron depends only on the angle between its initial and final direction. The position and results of succeeding collisions are found by repeating the above procedure for each flight and collision of the neutron. The neutron trajectory is traced until the neutron is emitted from a collision with an energy lower than the lower bound of the energy region of interest. The sum of these final weights, divided by the total of the initial weights for all neutrons, is the resonance-escape probability for the energy region considered. Similarly, the sums of the contributions of the individual neutrons to the absorption and fission probabilities in each hypercube of phase space, divided by the total of the initial weights of all neutrons, are the absorption and fission probabilities in each hypercube.

### 2. Determination of the Absorption Probability and Statistical Error

At each collision point, $\overline{X}_i$, the quantity

$$A_i = W_i \Sigma_{ai} / \Sigma_{Ti} \tag{154}$$

is tabulated as a contribution to the absorption probability, as mentioned in Section I above. To determine the probable error in the final estimate of the absorption probability, the quantity $A_i^2$ is also tabulated. After an arbitrary (input) number of neutron histories have been traced, the absorption probability is determined according to the general theory formulated in Section II-A. Explicitly, the absorption probability is

$$P_{abs} = \frac{1}{N_p} \sum_i \frac{A_i}{K}, \tag{155}$$

where the summation is over all collision points, $N_p$ is the total number of collision points, and K is the required normalization factor. Since the expected value of the neutron starting weight is $\langle W_0 \rangle = 1$, the normalization factor could be taken as $N/N_p$, where N is the number of histories. This was commonly done in earlier Monte Carlo work. However, the average value of the starting weights of any finite number of neutrons is different from the expected value. This difference, which is a random variable, introduces additional variance in the computed value of the absorption probability when $N/N_p$ is used as the normalization factor. This additional statistical error is avoided by taking $K = W_{total}/N_p$, where $W_{total}$ is the total of all initial neutron weights.

The fission probability is determined in a manner precisely analogous to that used to determine the absorption probability.

Similarly, the variance is computed from the tabulated values of $A_i$ and $A_i^2$, using the formula

$$\sigma^2 = \left[ \frac{1}{N_p} \sum_i \left( \frac{A_i}{K} \right)^2 - \frac{1}{N_p^2} \left( \sum_i \frac{A_i}{K} \right)^2 \right] \frac{1}{N_p}$$

$$= \frac{1}{W_{total}^2} \left[ \sum_i A_i^2 - \frac{1}{N_p} \left( \sum_i A_i \right)^2 \right]. \tag{156}$$

The probable error is 0.67449 times the standard deviation, $\sigma$.

### 3. Geometric Techniques for the Full-core Calculations

To achieve some economy in fabrication, reactor cores are commonly designed as repeating arrays of identical components. Therefore, the reactor core can be represented for nucleonics analysis as a composite of identical unit cells. Typically, the fuel rods are arranged in either a square or a hexagonal pattern, with the hexagonal pattern usually preferred because it results in better coolant circulation.

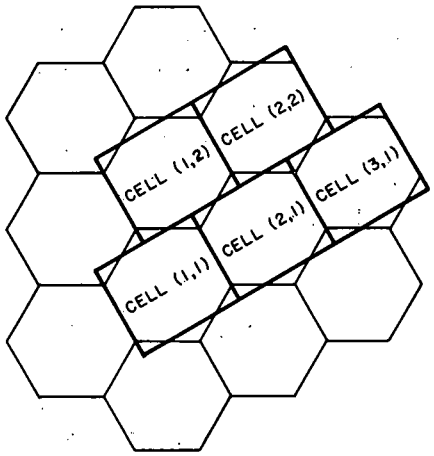


Fig. 1. Equivalent Hexagonal and Rectangular Cells

To facilitate the development of the geometric algorithms, hexagonal arrays are considered to be composed of appropriately constructed rectangular cells. The arrangement of fuel, cladding, and moderator is represented exactly in the rectangular cells. The rectangular boundaries are a calculational convenience and have no effect on the accuracy of the result. (See Fig. 1.) The neutron position is defined by the indices of the cell in which it is located, and by its Cartesian coordinates relative to the center of that cell. After each neutron flight, the neutron coordinates relative to the center of the cell of its previous collision (real or fictitious; see Section II-C) are transformed to coordinates relative to the center of the cell of its latest collision. Simultaneously, the cell indices of the latter cell are determined. Keeping the neutron coordinates relative to the cell containing the neutron simplifies the tests for determining in which region of the cell the neutron is located. This information is necessary to find the flight-path length by the fractional interaction technique, described in Chapter II. Also, the region and cell containing the neutron at each collision must be known in order to compute the absorption and fission probability in each isotope in each spacial region of each cell.

4. Tabulation of Results

The absorption and fission probabilities in each isotope are computed as a function of the cell indices (x and y), the spacial region of the cell, the energy region, and the characteristic dimension of the cell. Also, the absorption and fission probabilities are computed as integrals over:

a. All isotopes, all spacial regions, and all cells.

b. All cells.

c. All isotopes, all spacial regions, all cells, and all energy regions.

Finally, the resonance-escape probability and the slowing-down densities at the lower limit of the energy range of interest are computed.

## B. Verification of the Theory and Techniques

To verify the accuracy of the coding and the reliability of the detailed algorithm encompassing the theory and techniques described in

Chapters II and III, numerical calculations were performed with the AMC code to test each section of the code. Some of these tests are enumerated and described here.

1. Homogeneous Resonance-integral Test

The resonance integral for an element with a single narrow resonance uniformly distributed in a highly moderating, weakly absorbing medium can be well approximated by the homogeneous, narrow-resonance theory of Wigner. Therefore, such a system was prescribed and the absorption probability was calculated using the AMC code. The result was compared with a separate hand calculation based on the narrow-resonance approximation. The parameters used in the comparison calculations were

Total width, $\Gamma$ = 0.5 eV;

Capture width, $\Gamma_\gamma$ = 0.2 eV;

Neutron width, $\Gamma_n$ = 0.3 eV;

Resonance energy, $E_0$ = 100 eV;

Potential-scattering cross section per absorber atom, $\sigma_p = 2 \times 10^6$ barns/atom;

and

Average logarithmic energy decrement, $\xi$ = 0.158.

The effective resonance integral is defined by the equation

$$I \equiv \int_{E_1}^{E_2} \frac{\Sigma_p \sigma_a(E)}{\Sigma_t(E)}\, dE, \tag{157}$$

where

$\sigma_a$ = microscopic absorption cross section,

$\Sigma_p$ = macroscopic potential-scattering cross section,

and

$\Sigma_t$ = macroscopic total cross section.

The resonance-escape probability is defined by[62]

$$P_{esc} \equiv \exp\left(-\int_{E_1}^{E_2} \frac{\Sigma_a}{\xi \Sigma_t} \frac{dE}{E}\right)$$

$$= \exp\left(-\frac{1}{\xi \sigma_p} I\right).$$

For $I \ll 1$, this is approximately

$$P_{esc} = 1 - \frac{1}{\xi\sigma_p} I. \tag{159}$$

The probability that a neutron will be absorbed in slowing through the energy region of the resonance is, therefore,

$$P_{abs} = 1 - P_{esc} = \frac{1}{\xi\sigma_p} I. \tag{160}$$

In the narrow-resonance approximation, the effective resonance integral, I, is given by[62]

$$I \approx \frac{\pi\sigma_0\Gamma\gamma}{2E_0}\left[1 + \frac{\sigma_0}{\sigma_p}\right]^{-1/2}, \tag{161}$$

where

$\sigma_0 = \frac{4\pi\lambda\!\!\!^{-}\,\Gamma_n}{\Gamma}$ = peak value of the resonance,

$\lambda\!\!\!^{-} = \frac{\lambda}{2\pi}$ = reduced neutron wavelength,

$\lambda = h(2\mu E)^{-1/2} = h/\mu V$,

h = Planck's constant,

$\mu$ = reduced mass of neutron,

V = neutron velocity,

and

$E = 1/2\ \mu V^2$,

or

$$\sigma_0 = \frac{2.6 \times 10^6 \Gamma_n}{E\Gamma}.$$

The value of the absorption probability computed using the AMC code was $(1.49 \pm 0.03) \times 10^{-4}$; the narrow-resonance approximation gives $1.52 \times 10^{-4}$.

In addition to verifying this integral result, the accuracy of many subsidiary calculations was verified. For example, cross sections and their temperature derivatives, geometric areas, and the distribution in energy and space of the source neutrons were compared with hand calculations.

2. Resonance Integral Test for Multiregion Problems

To test additional parts of the code, a problem with two spatial regions and two energy regions was specified. Both spatial regions contained the same material that was specified for the first problem. The energy range of the calculation was divided into two regions, one above and one below the energy of the resonance peak. The set of random numbers used in the first problem was also used for this problem, and the same value for the effective resonance integral was obtained. Since the resonance is narrow, compared to the average energy loss in a scattering collision, the flux is nearly constant over the resonance. Therefore, a symmetrical absorption cross section should result in approximately equal absorption above and below the energy of the resonance peak. As expected, the calculated absorption probabilities in the two regions were within 1% of being equal. Also, as expected, the absorption probabilities in the spatial regions were proportional to the volumes of the spatial regions, verifying the accuracy of the multiregion calculation.

3. Test of Full-core Calculation

The AMC code can consider a full reactor core composed of any number of identical cells. To test this option, a test problem was devised using 25 cells, each composed of two regions identical to those of the previous test problem. The cells were surrounded by a perfect reflector. The correct resonance integral was again obtained.

4. Test with Two Resonance Absorbers with Two Resonances Each

The AMC code can consider any number of resonance absorbers, each having any number of resonances, limited only by the dimension statement used. To verify the accuracy of the algorithm used, the calculation was performed with two identical resonance absorbers, each having two identical resonances like the resonances considered in the first test problem. The absorption probabilities computed for each resonance were identical for the resonances at the same energy, and within 1% for resonances at different energies.

5. Test of Perturbation Technique for Temperature Derivative Calculations

A series of seven problems was run to test the ability of the code to calculate the temperature derivatives of the reaction rates. The

results of this series of calculations are tabulated in Table I. The table indicates the accuracy of the perturbation technique. Comparison of the third and fifth columns shows that the change in the absorption probability per degree computed by the perturbation technique agrees with the temperature derivative computed from the results of two problems for different temperatures.

TABLE I. Results of Test of Temperature-perturbation Method

| Temperature, °K | Absorption* Probability x $10^{2}$** | $\delta A/\delta T \times 10^{5}$, $°K^{-1}$ | Derivative* x $10^{5}$, $°K^{-1}$ | Average Derivative x $10^{5}$, $°K^{-1}$ |
|---|---|---|---|---|
| 100 | 3.33 ± 0.12 | | 4.93 ± 0.25 | |
| | | 3.48 ± 0.70 | | 3.26 ± 0.14 |
| 350 | 4.20 ± 0.13 | | 2.58 ± 0.11 | |
| | | 2.12 ± 0.76 | | 2.18 ± 0.06 |
| 600 | 4.73 ± 0.14 | | 1.77 ± 0.07 | |
| | | 1.56 ± 0.79 | | 1.56 ± 0.04 |
| 850 | 5.12 ± 0.14 | | 1.39 ± 0.05 | |
| | | 1.28 ± 0.79 | | 1.28 ± 0.03 |
| 1100 | 5.44 ± 0.14 | | 1.16 ± 0.04 | |
| | | 1.08 ± 0.79 | | 1.08 ± 0.02 |
| 1350 | 5.71 ± 0.14 | | 1.00 ± 0.03 | |
| | | 0.89 ± 0.82 | | 0.89 ± 0.02 |
| 1850 | 6.15 ± 0.15 | | 0.78 ± 0.03 | |

*The absorption probability, A, is defined as the fraction of the neutrons that enter the energy region considered that are absorbed in this energy region. The absorption probability and its derivative are computed directly by the AMC code. The other two columns are derived from the computed quantities and are directly comparable.

**The absorption probability is the tabulated number times $10^{-2}$; the derivatives are the tabulated numbers times $10^{-5}$.

### 6. Test of the Variational Method for Calculation of Rod-size Effects

Two types of problems were run to test the variational method used to obtain reaction rates in systems with different characteristic dimensions. The first problem was chosen to minimize the effect of a change in the fuel diameter. This was accomplished by choosing cross sections and dimensions so the mean free path of the neutron extended through several fuel rods. Thus, the probability that a neutron will have successive collisions in fuel regions is little affected by a change in the diameter of the fuel rods. The deviations in the results are an indication of the variance that results from the method of calculation. As shown in Table II, the error depends upon the fractional change in rod size considered. The 1-cm rod is considered the base case. For a 25% perturbation (0.75-cm rod), errors of 0.1% in the absorption probability and 2% in its derivative were obtained. The results for changes larger than 25% are unsatisfactory. From these results, it is concluded that variations of rod size of more than 25% should be treated by running a series of problems with a size difference of 25% between successive problems.

TABLE II. Results of First Test of Fuel Rod-size Variation Calculation

| Radius of Fuel Rod, cm | Absorption Probability x $10^2$* | % Error | $\partial A/\partial T \times 10^6$ °K$^{-1}$ | % Error | Obtained by |
|---|---|---|---|---|---|
| 1.00 | 0.01666 | - | 2.91 | - | Direct calculation |
| 0.75 | 0.01658 | 1 | 2.86 | 2 | Variation calculation |
| 0.50 | 0.0172 | 3 | 3.10 | 6 | Variation calculation |
| 0.25 | 0.0175 | 5 | 3.69 | 26 | Variation calculation |

*The absorption probability, A, is the tabulated number times $10^{-2}$.

The second type of problem was designed to have a large rod-size effect. The results tabulated in Table III show that a large effect was indeed obtained, and that the technique gave results very close to the results obtained by direct calculation for variations of 25%.

TABLE III. Results of Second Test of Fuel Rod-size Variation Calculation

| Radius of Fuel Rod, cm | Absorption Probability, A | $\partial A/\partial T \times 10^5$,* °K$^{-1}$ | Obtained by |
|---|---|---|---|
| 1.00 | 0.158 ± 0.004 | 0.80 ± 0.07 | Direct calculation |
| 0.75 | 0.205 ± 0.004 | 1.07 ± 0.08 | Variation calculation |
| 0.75 | 0.203 ± 0.004 | 1.11 ± 0.07 | Direct calculation |
| 0.50 | 0.224 ± 0.009 | 1.37 ± 0.15 | Direct calculation |

*$\partial A/\partial T$ is the tabulated number times $10^{-5}$.

## 7. Comparison with Other Numerical and Monte Carlo Methods

The next test involved a problem of considerably greater complexity. It consisted of a two-region cell with one resonance absorber and two scattering isotopes in the central region, and with four scattering isotopes in the outer region. The resonance parameters for the 25 resonances of $U^{238}$ between 1 and 1.4 keV were used.[34] This problem was selected so as to be within the range of applicability of two existing numerical techniques[56,57] and the RECAP II Monte Carlo code.[15]

The techniques used in the AMC code are quite different from the standard Monte Carlo techniques used in the RECAP II code. In particular, the fractional interaction technique used in the AMC code represents an entirely different geometric method than the standard method used in the RECAP II code. Furthermore, different sets of random numbers were used in the two Monte Carlo calculations. However, both programs treat the transport process correctly without approximations at the boundaries and, therefore, arrive at the same value for the absorption probability.

The absorption probabilities computed by the numerical techniques differ from the Monte Carlo results by 5 and 13%, as shown in Table IV.

TABLE IV. Comparison of Results from Four Computational Methods
(Two-region cell with 25 resonances in Region 1)

| Program Name | T, °K | Absorption Probability x $10^2$** | $\delta A_{500-1100°K} \times 10^2$ | Reference |
|---|---|---|---|---|
| AMC | 500 | 1.23 ± 0.03 | - | - |
| RECAP II | 500 | 1.23 ± 0.04 | - | 15 |
| RABBLE | 500 | 1.31 | - | 57 |
| RIFF RAFF | 500 | 1.393 | - | 56 |
| AMC | 1100 | 1.35 ± 0.04 | 0.122 ± 0.004* | - |
| RIFF RAFF | 1100 | 1.564 | 0.17 | 56 |

*Determined from derivatives at 500 and 1100°K.
**The absorption probability is the tabulated number times $10^{-2}$.

The temperature derivative of the absorption rate computed directly by the AMC code is in agreement with the temperature derivative obtained from the absorption rates computed by the AMC code at 500 and 1100°K. The difference in the absorption rates at 500 and 1100°K is shown in the fourth column of Table IV. The value computed by one of the approximate numerical methods differs from the AMC Monte Carlo result by 40%.

The variation in the results gives some indication of the errors due to the assumptions necessary in the numerical techniques. (See Chapter I.)

# CHAPTER IV

# VERIFICATION OF THE THEORY BY COMPARISON WITH EXPERIMENTS

## A. Rod-size Tests in a Critical Facility

### 1. Description of the Experiment

The Doppler coefficient of uranium in a large plutonium-uranium carbide fast-reactor composition has been measured by heating uranium oxide fuel rods of two different diameters.[33] The experiments were performed on the ZPR-3 reactor shown in Fig. 2. The ZPR-3 reactor is a zero-power critical facility designed and operated by the Argonne National Laboratory.[19] The plutonium-uranium carbide composition was constructed of plates of separate materials held in 2-in.-sq stainless steel drawers, supported in turn by a square matrix of stainless steel tubes. A device for holding the uranium Doppler sample, surrounded by heater wires

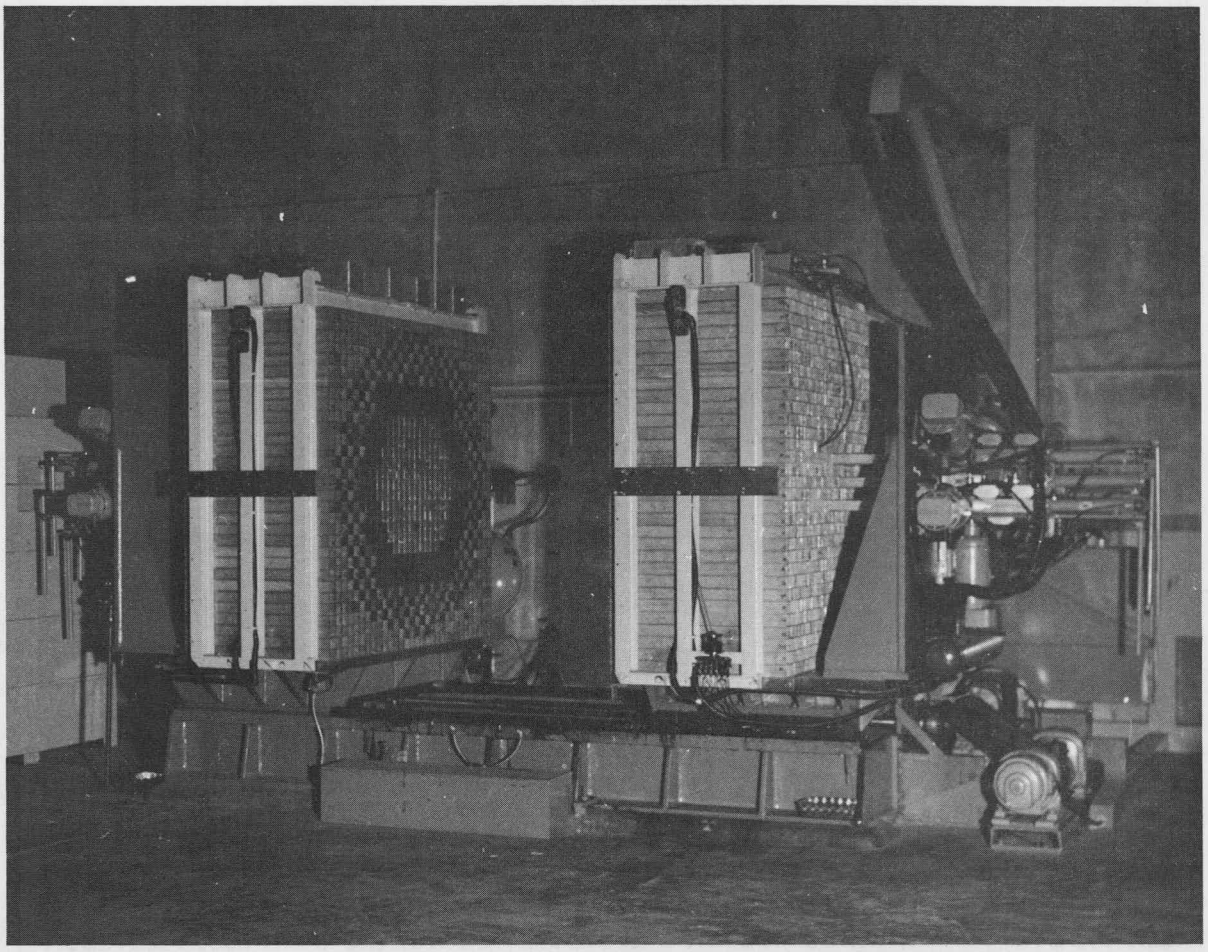

103-298

Fig. 2. ZPR-3 Critical Facility

and sealed in a vacuum jacket, is inserted in one of the matrix tubes. The construction of the Doppler element is shown in Fig. 3. The reactivity worth of the Doppler sample is measured relative to the worth of a reference sample of the same composition by alternately placing the Doppler sample and the reference sample in the center of the core and recording the position of an automatic control rod, which maintains the system at criticality. The Doppler sample is then heated by means of the heater wires, and the measurement is repeated. The change in the reactivity worth of the Doppler sample is found by subtracting the worth of the unheated Doppler sample relative to the reference sample from the worth of the heated Doppler sample relative to the reference sample. The reference sample is made as nearly identical to the Doppler sample as possible, so that the reactivity variation, when samples are interchanged, is minimized. Thus a more sensitive control rod can be used, and a more precise measurement of the change in reactivity when the Doppler sample is heated is obtained.

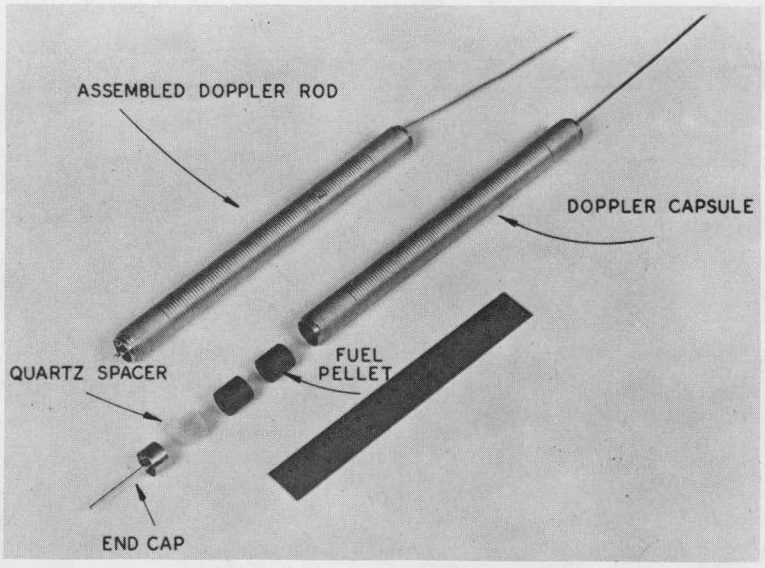


112-5704

Fig. 3
Doppler Element

## 2. Mathematical Model

The mathematical model used for the comparison calculation accurately described the geometry and composition of the experiment in the region of the temperature perturbation and within about 30 mean free paths of the perturbed region, as shown in Fig. 4 and Table V. Specifically, four concentric cylindrical regions, infinite in height, were considered: the uranium-oxide rod, the vacuum jacket and structural materials, a thin scattering zone surrounding the Doppler equipment, and a fuel zone containing the plutonium-uranium carbide fast-reactor composition. The uranium oxide rod contained depleted uranium, combined stoichiometrically with oxygen and sintered to 70% of theoretical density. The vacuum jacket, heater wires, and support structure filled the surrounding space with iron,

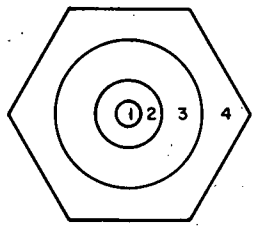


REGION

1 DOPPLER ELEMENT-DEPLETED URANIUM OXIDE

2 HEATER, VACUUM JACKET, AND STRUCTURE

3 SCATTERING ZONE-GRAPHITE AND IRON

4 FUEL ZONE - PLUTONIUM, URANIUM, SODIUM, ETC.

Fig. 4. Geometry and Composition for Rod-size Experiment

nickel, and chromium with atomic densities, respectively, of 0.0127, 0.0018, and 0.0046 ($10^{-24}$ atoms/cc). The scattering zone containing carbon was used in the experiment to eliminate interference between the resonances in the Doppler sample and the core. The surrounding core volume containing thin plates of uranium, plutonium, sodium, and graphite were represented in the calculation as a homogeneous mixture. The Doppler sample is located near the center of the core where the gradient of the flux is small. Therefore, zero net current was assumed at a boundary 5 cm from the Doppler sample, and a reflecting boundary condition was used.

The energy range from 29 eV to 9.1 KeV was considered. This is the energy range that produces the Doppler effect. Near the top of this energy range, the resonances overlap so strongly, even at room temperature, that a further increase in temperature does not result in an increased absorption rate. Near the bottom of this range, the neutron flux is so small that any change in the cross sections is not important. Neutron histories are traced in this region of phase space in which the Doppler effect occurs, and the temperature derivatives of the absorption and fission rates are computed as described in Chapters II and III.

TABLE V. Isotopic Compositions for Rod-size Experiment

| Region | Composition | atoms/ barn-cm |
|---|---|---|
| 1 | $U^{238}$ | 0.0156 |
| | $U^{235}$ | 0.0001 |
| | Oxygen | 0.0314 |
| 2 | Iron | 0.0127 |
| | Nickel | 0.0018 |
| | Chromium | 0.0046 |
| 3 | Carbon | 0.0354 |
| | Iron | 0.0257 |
| | Nickel | 0.0036 |
| | Chromium | 0.0069 |
| 4 | $U^{238}$ | 0.0075 |
| | $Pu^{239}$ | 0.0014 |
| | Iron | 0.0118 |
| | Nickel | 0.0016 |
| | Chromium | 0.0032 |
| | Sodium | 0.0107 |
| | Carbon | 0.0057 |

### 3. Results and Conclusions

The calculation with the AMC code determines the fractional change in the fission rate in the region of phase space considered. This must be multiplied by the fraction of fissions in the reactor that take place in the region of phase space considered, in order to obtain the temperature coefficient of reactivity. Using a value for the latter quantity determined by multigroup methods, the computed Doppler coefficients differed from the measured values by 10%. Of more

significance to this work is the ratio of the Doppler coefficients per unit mass, of the 0.5-in. uranium oxide rod and the 1-in. rod. This ratio is independent of the fraction of total fissions occurring in the region of phase space considered in the calculation with the AMC code and is obtained directly from the results obtained with the AMC code. The computed value of this ratio was $1.16 \pm 0.03$. The measured value was $1.19 \pm 0.03$. This agreement is considered quite satisfactory. Detailed results are shown in Table VI.

TABLE VI. Variation of Doppler Coefficient with Diameter of Doppler Element

| | Computed | Measured |
|---|---|---|
| Fraction of fissions in the reactor that occur in the region of phase space considered | 0.0072 | |
| Fractional change in the fission rate in the region of phase space considered: | | |
| 0.5-in. rod | $-1.83 \times 10^{-6}$ | |
| 1.0-in. rod | $-6.30 \times 10^{-6}$ | |
| Doppler coefficient per unit mass (computed at 500°K; measured 500-1100°K) | | |
| 0.5-in. rod | $-4.54 \times 10^{-8}$ | $-4.62 \times 10^{-8}$ |
| 1.0-in. rod | $-3.91 \times 10^{-8}$ | $-3.88 \times 10^{-8}$ |
| $\frac{\text{Doppler coefficient per unit mass of 0.5-in. rod}}{\text{Doppler coefficient per unit mass of 1.0-in. rod}}$ | $1.16 \pm 0.03$ | $1.19 \pm 0.04$ |

## B. Tests with Various Materials Surrounding the Doppler Sample

Experiments have been performed in which the material surrounding the Doppler sample was varied and the Doppler coefficient determined as a function of the surrounding material.[17] The experiments indicated that the measured Doppler coefficient depended significantly on the material surrounding the Doppler element.

Since this phenomenon results from the complex variation of the neutron cross sections with temperature, space, and neutron energy, these experiments were chosen as the basis for a final test of the theory and techniques used in the AMC code. The experimental configurations and techniques were similar to those used in the rod-size test described above, and the mathematical model was chosen in the same manner. The Doppler region was a 1.125-cm-diam circular cylinder of thorium metal. The Doppler element was surrounded by a 0.635-cm annulus of 25% iron,

75% void, to represent the heater and heat shields. This, in turn, was surrounded by a 0.95-cm-thick blanket region of void, thorium metal, or uranium metal. The outer region contained core material of 15 v/o $U^{238}$, 15 v/o $U^{235}$, 15 v/o iron, and 55 v/o sodium. Figure 5 shows the geometry and composition used.

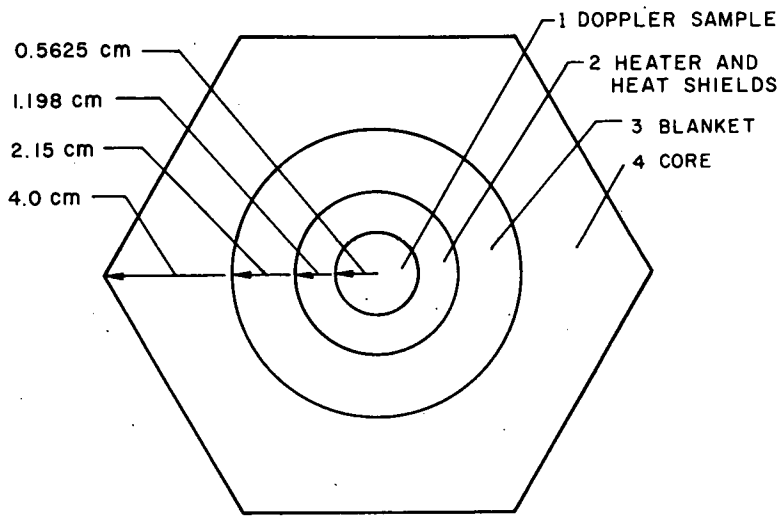


| REGION | VOLUME | FRACTIONS |
|---|---|---|
| 1 | Th | 1.00 |
| 2 | Fe | .25 |
| | VOID | .75 |
| 3 | Th, U, OR VOID | 1.00 |
| 4 | Na | .55 |
| | Fe | .15 |
| | U-238 | .15 |
| | U-235 | .15 |

Fig. 5. Geometry and Composition Used in Study of Effect of Surrounding Material on the Doppler Coefficient

TABLE VII. Relative Doppler Coefficient of a 1.125-cm Thorium Fuel Element Surrounded by Various Blankets

| Blanket | Relative Value of $\partial A/\partial T/A$ Computed | Relative Doppler Coefficient Measured[17] |
|---|---|---|
| Void | 1.00 | 1.00 |
| Thorium | 1.13 | 1.25 |
| Uranium | 0.77 | 0.79 |

Table VII shows the results of the experiment and calculation. The theoretical results agree at least qualitatively with the experiment. Surrounding the thorium Doppler sample with a thorium blanket increases the measured Doppler coefficient. Surrounding it with a uranium blanket decreases the Doppler coefficient. The estimated error in both the experimental and theoretical results is ±4%. The discrepancy between the experimental and theoretical results is slightly outside this range for the thorium blanket, but well within this range for the uranium blanket.

# CHAPTER V

# THE EFFECT OF HETEROGENEITY ON THE DOPPLER COEFFICIENT OF A LARGE FAST REACTOR

## A. Description of Reactor

The accuracy of the theory and techniques described in Chapters II and III, having been verified by comparison with known solutions to simple problems and by comparison with experiments, the study was extended to investigate the effect on the Doppler coefficient of changing the size of the fuel rods in an advanced fast power reactor.

Nuclear power stations now under design and construction in the United States typically have an electrical power capacity of about 1000 MW. The first economical fast reactors will probably also be about this size. Therefore, recent fast-reactor design studies have concentrated on this size reactor. For the present work, a 1000-MW fast-reactor design proposed by the Atomic Power Division of the Westinghouse Electric Corporation[84] was taken as the reference design, and the possibility of enhancing the Doppler coefficient by reducing the size of the fuel rods was investigated.

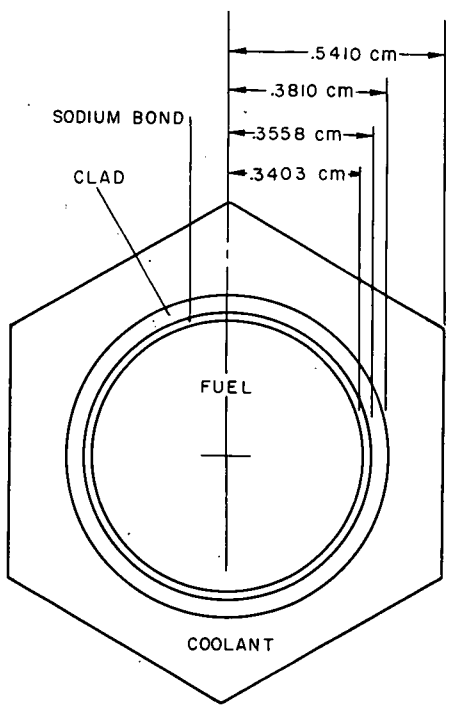


| REGION | COMPOSITION (ATOMS/ b-cm) | |
|---|---|---|
| 1 | U-238 | .02499 |
| | Pu-239 | .00441 |
| | C | .02940 |
| 2 | Na | .02160 |
| 3 | Fe | .08520 |
| 4 | Na | .02160 |

Fig. 6. Unit Cell of 1000-MW Westinghouse Reactor

The core is composed of stainless-steel-clad plutonium-uranium-carbide fuel rods surrounded by sodium coolant. Sodium also fills the gap between the fuel and cladding. Figure 6 shows the dimensions of a unit cell of the core, composed of a fuel rod and a proportionate part of the coolant associated with one fuel rod. Figure 6 also indicates the atomic composition. The nominal enrichment of the fuel is 15%.

## B. Mathematical Model

Since the reactor under consideration is very large and contains thousands of fuel elements, a unit cell calculation should provide an accurate description of the phenomenon involved. The cell indices, then, may be dimensioned for a maximum of one, leaving adequate computer memory available for the treatment of other variables. This memory space was utilized to store resonance parameters for 11 plutonium resonances and 215 $U^{238}$ resonances that have been resolved,[38] and for 109 additional plutonium resonances and 145 additional

$U^{238}$ resonances selected from the appropriate statistical distributions[73] in the unresolved regions. The heterogeneous arrangement of fuel, bond, cladding, and coolant was represented exactly. The entire energy region from 100 eV to 30 keV in which the Doppler effect occurs was considered.

C. Results

The Doppler coefficient (D.C.) is defined as the logarithmic derivative with respect to temperature of the multiplication constant, due to resonance broadening; i.e.,

$$D.C. = \frac{1}{K}\frac{\partial K}{\partial T}, \tag{162}$$

where

$T$ = temperature,

and

$K$ = the multiplication constant.

The effect of a temperature perturbation in the core is to modify the neutron cross sections in the region of phase space, R, where R encompasses the volume of the core and the energy range, $0 < E < 30$ keV. The region, R, is chosen sufficiently large that $\partial F/\partial T = 0$ outside of R, where F is the fission rate. Then

$$\frac{\partial F_R/\partial T}{F_R} \cdot \frac{F_R}{F_t} = \frac{\partial F_t/\partial T}{F_t} = \frac{\partial K/\partial T}{K} = D.C., \tag{163}$$

where

$F_R$ = fission rate in R,

and

$F_t$ = total fission rate.

The factor $(\partial F_R/\partial T)/F_R$ is obtained from the Monte Carlo calculation; the factor $F_R/F_t$ is obtained to sufficient accuracy by the faster ELMOE calculation.[74] In the present case, the factor $(\partial F_R/\partial T)/F_R$ was computed to be 0.18, and the factor $(\partial F_R/\partial T)/F_R$ was found to be $-8.89 \times 10^{-5}/°C$. This leads to a Doppler coefficient of $-1.60 \times 10^{-5}\,\Delta K/K/°C$, which is about 10% less than the number reported in the original design report.[84]

Changing the fuel-rod size and pitch both by the same factor leaves the average composition of the core unchanged. The fractional change in fission rate per degree for a reactor with fuel rods of half the reference size and pitch, 0.3 cm OD, 0.43 cm OC, was computed by the AMC code to be $-10.0 \times 10^{-5}$. This leads to a Doppler coefficient of $-1.8 \times 10^{-5}$ $\Delta K/K/°C$. The ratio of the Doppler coefficient in the system with the small fuel rods to the Doppler coefficient in the system with the larger fuel rods is therefore $1.13 \pm 0.03$. This result is independent of the ratio $F_R/F_T$, and is obtained directly from the AMC results.

Despite the fact that the problem investigated here is quite different from the question of what happens when the diameter of a single rod in the center of a critical assembly is varied, the result is nearly the same. In the case of the critical assembly, reducing the diameter of the Doppler rod by 1/2 resulted in an increase in the Doppler coefficient per unit mass of 16 to 19%. Here a decrease in the diameter of the fuel rods by a factor of 1/2 results in an increase in the Doppler coefficient of 13%, which is an effect of the same order of magnitude and in the same direction. This effect, although significant, is not sufficiently large to override other considerations, such as heat-transfer and fabrication costs. Nonetheless, it does provide incentive for reducing the fuel-rod size in addition to the incentive provided by the desirability of increasing heat-transfer rates. These considerations may influence reactor designers toward a preference for smaller fuel rods.

# CHAPTER VI

# SUMMARY

## A. Summary of the Present Work

This work has developed a theoretical method for the analysis of the Doppler effect and applied the method to determine the effect of the size of the fuel elements on the Doppler coefficient of a typical fast breeder reactor.

In the development of this method, particular emphasis was placed on the elimination of the approximations and assumptions that have limited the accuracy and reliability of previous methods. This required the development of several additions to Monte Carlo theory; specifically,

1. The temperature derivative of the absorption rate was formulated as an integral involving the collision density times a function of the neutron cross sections. The latter function is a temperature-derivative estimator that involves the neutron cross sections only at the collision points, eliminating the integral over the neutron flight path in the temperature-derivative estimator previously used.

2. A technique was developed for determining the variation of the Doppler coefficient when the size of the fuel elements in a fast reactor is changed without changing the fuel and coolant volume fractions.

3. A rigorous mathematical theory was formulated for a technique that eliminates the calculation of optical distances from the point of each collision to each region boundary point through which the neutron passes on its way to the next collision.

4. A technique was developed that permits a more versatile description of the energy distribution of the neutrons scattering into the resonance region.

5. The continued-fraction expansions of the Doppler broadening functions suggested by O'Shea and Thacher[72] were adapted to provide fast and accurate evaluation of the neutron cross sections at each neutron energy.

The theoretical method developed by combining these theories into a consistent algorithm was used as the basis for the AMC digital-computer program. In addition to the speed and accuracy provided by these new techniques, the program has the advantage of considerable generality. For example, it can be applied to determine the effect of temperature perturbations that occur either throughout the core or in a single cylindrical region.

The program was checked by comparing the resonance integral for a simple case computed by the program with the resonance integral determined by analytic methods known to be valid for the simple case considered. Further tests involved comparisons of the resonance escape probabilities computed for cases within the capabilities of the RIFF RAFF, RABBLE, and RECAP II codes. The similarity of results corroborated the reliability of the AMC program. Finally the program was checked by comparison with Doppler experiments performed in critical assemblies. In each case, the agreement with the experimental results was good, further corroborating the reliability of the theory and the AMC program.

The program was then used to determine the effect on the Doppler coefficient of varying the size of the fuel elements in a typical fast breeder reactor. Reducing the diameter of the fuel elements by one-half, and reducing the pitch of the lattice by one-half to maintain the same volume fractions in the core, would increase the Doppler coefficient by 13%.

B. Possible Future Applications

The theory developed in this research and incorporated into the AMC program constitutes an efficient procedure for handling geometrical data, computing cross sections, tracing neutron histories, and tabulating the results. In its present form, the program is applicable to a wide range of neutron-transport problems such as the one investigated in the present research. By modifying these procedures or building upon the framework provided, one can analyze many additional problems that arise in the design of fast reactors, e.g., determining the sodium-void coefficient.

With the present version of the program, the effect on the measured Doppler coefficient of varying the material surrounding the heated sample in a Doppler experiment will be studied further.

One planned application of the AMC program is the investigation of the error introduced into earlier numerical methods by various theoretical approximations. For example, the assumption used in the advanced resonance integral code RIFF RAFF that the flux crossing the boundaries between dissimilar materials is isotropic can be readily investigated using the AMC program. Many other previously used assumptions of a similar nature will also be investigated in the near future.

Although the AMC code, incorporating the theory developed in this research, has been found by direct comparison to be considerably more efficient than earlier Monte Carlo methods, the time required to obtain the answer for a complex problem is still considerable. For this reason it may be desirable to use faster (though approximate) multigroup methods for survey calculations. However, for these calculations to be meaningful,

one must have available correctly averaged group constants. With a slight modification, the AMC code will produce group constants appropriately averaged, taking into consideration a detailed description of the cross sections as a function of both energy and space.

Additional questions that should be investigated include the following:

1. The variation of the Doppler coefficient as a function of the ratio of fertile and fissile isotope atomic densities.
2. The variation of the Doppler coefficient as a function of the ratio of coolant and fuel volume fractions.
3. The variation of the Doppler coefficient with temperature.
4. The possibility of increasing the Doppler coefficient by adding isotopes to the core specifically for this purpose. For example, the effect of adding beryllium might be investigated.

# APPENDIX A

## Calculation of the Escape Probability for a Finite Cylinder

The physical system considered is a finite cylinder of scattering and absorbing elements, characterized by macroscopic cross sections $\Sigma_s$ and $\Sigma_a$. Neutrons enter the cylinder with isotropic angular distributions and are eventually absorbed or leave the system. It is required to determine the escape probability, defined as the fraction of neutrons that eventually escape from the cylinder.

In the Monte Carlo solution of this problem a direct physical analog is used, except for one deviation. None of the neutrons are absorbed. Instead an initial weight of one is assigned to each neutron. Then in each collision the weight is reduced by a factor of $\Sigma_s/\Sigma_t$. Thus, a fraction $\Sigma_a/\Sigma_t$ of the neutron is absorbed in each collision until the neutron escapes from the cylinder. The weight at the time of escape is the faction of the neutron that escapes. The average weight at the time of escape for 1000 neutrons is the escape probability.

Figure 7 shows the details of the calculation. The physical interpretations of the undocumented symbols used on the flow diagram are the following:

N = number of entering neutrons,

W = neutron weight, i.e., the fraction of the neutron not already absorbed,

WSUM = sum of the neutron weights at time of escape from the cylinder,

L = number of neutron histories processed between printouts of results,

$\Sigma_s$ = macroscopic scattering cross section,

$\Sigma_t$ = macroscopic total cross section,

$\Sigma_a$ = macroscopic absorption cross section,

A = fractions of neutrons absorbed,

A = absorption probability (in print statement),

and

ESP = escape probability.

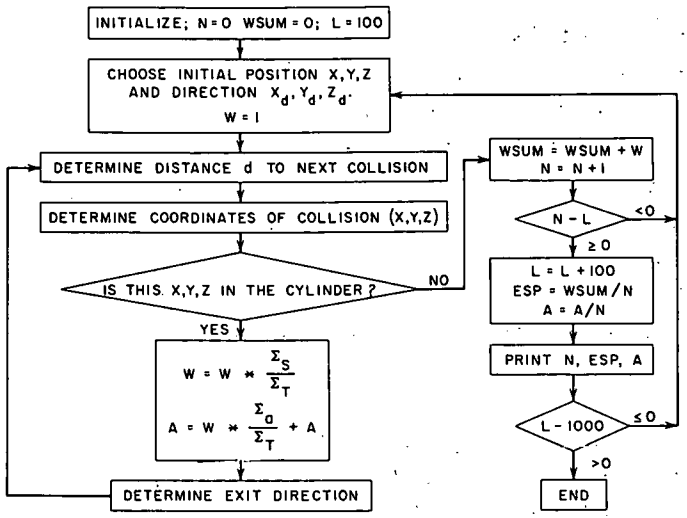


Fig. 7
Calculation of Absorption Probability in a Finite Cylinder

One neutron at a time is followed from the time it enters the rod until it escapes. The initial position of the neutron is taken to be at $y = 0$, $x = 1$, with no loss of generality since the properties of the rod and the intensity of the incident flux are assumed to be independent of the azimuthal angle. The axial coordinate, $z$, is chosen from a uniform distribution on the interval, $[0, \ell]$, where $\ell$ is the length of the cylinder. Operationally, $z$ is computed from the equation

$$z = \ell\rho, \tag{164}$$

where $\rho$ is a random number chosen from a uniform distribution on the interval $[0, 1]$.

The initial direction is chosen from an isotropic distribution of all possible incident directions by choosing a set of three random numbers for which $\rho_1^2 + \rho_2^2 + \rho_3^2 < 1$, and $\rho_2 < 0$. The direction $\overline{\Omega}$ along a line drawn from the origin through the point $(\rho_1, \rho_2, \rho_3)$ is taken as the initial direction of the neutron.

Next, the distance the neutron travels before its first collision is determined from the equation

$$d = -\frac{1}{\Sigma_t} \ln \rho. \tag{165}$$

Having determined the neutron's initial position and direction, and the distance to its first collision, the program determines the point of collision by trigonometry. If the point of collision is in the cylinder, the neutron weight is adjusted as previously explained, and the contribution to the absorption estimate for this sample point is computed.

The exit direction is determined from an isotropic distribution, and the distance to the next collision is again determined from Eq. 165.

The neutron history is traced in this way until a collision occurs outside the cylinder. At this time the neutron has escaped and its weight is added to the sum of the weights of preceding neutrons. This sum divided by the number of neutrons processed is the escape probability. Similarly, the absorption probability is the sum of the individual contributions to the absorption estimator divided by the number of neutrons processed. These quantities are computed and printed after every 100 neutron histories, and the calculation is terminated after 1000 histories. Determination of the absorption probability in this way for a given cylinder size and composition requires about 5 sec on the CDC-3600 computer.

If the number of incident neutrons per unit solid angle is proportional to cos $\theta$, where $\theta$ is the angle between the incident neutron direction and the normal to the surface of the cylinder, we can still choose the starting direction of each neutron from an isotropic distribution if we assign to each neutron a starting weight of

$$W = \cos \theta. \tag{176}$$

The escape probability is then the sum of the final weights divided by the sum of the initial weights.

By using this technique we can obtain the escape probabilities for any number of incident angular distributions from one set of neutron histories. It is only necessary to keep track of one weight for each neutron for each angular distribution.

# APPENDIX B

## Calculation of Multiregion, Hot-Cold Interference Effects

### A. Introduction

What influence, if any, the unheated material surrounding the heated element in a Doppler-coefficient measurement has on the measured reactivity is a question that has been investigated and discussed by theoretical and experimental reactor physicists for several years. Storrer et al.[86] concluded, theoretically, that the Doppler coefficient of a sample could be measured to first order if the surrounding core was composed of the same material as the sample. They further concluded that the Doppler coefficient could be measured to first order, even if the sample composition is different from that of the surrounding medium, provided that the sample is "very small."

Experiments at Argonne[91] showed no significant change in the Doppler coefficient as the material surrounding the Doppler element was varied. However, later measurements by Carpenter et al.[17] at Atomics International, with the sample blanketed by various materials, showed significant variations in the Doppler coefficient.

The usual analytic and numerical methods are inadequate to treat the rapid fluctuations of the neutron flux in space and energy that result from the heterogeneous arrangement of resonance absorbers in these experiments. Therefore, the new Monte Carlo program, AMC, was employed to calculate the space- and energy-dependent reaction rates and their derivatives with respect to the temperature of the Doppler sample, in the resonance region, for several exemplary cases.

Four cases of practical significance were investigated. The phenomena considered were:

1. The effect of "cold" resonances on the heated sample, with different resonance absorbers in the cold material and heated samples.

2. The effect of "cold" resonances on the heated sample, with the cold material containing the same resonance absorber as the sample.

3. The effect of separating the interacting resonance materials with nonresonant structural materials.

4. The effect of varying the thickness of the blanket surrounding the Doppler element.

The resonance parameters of Firk[34] were used for $U^{238}$ in the energy region 1.0 to 1.4 keV. The resonance parameters for thorium were taken from BNL-325.†

## B. AMC Calculations

### 1. Case 1: Doppler Element Surrounded by Different Resonance Material

To isolate the effect of the interaction of the broadened resonances in the Doppler element and the unbroadened resonances in the surrounding medium, four two-region problems were run. The Doppler region was a 1.125-cm-diam circular cylinder, surrounded by a cylinder of hexagonal cross section, 3 cm on a side. In all four problems, the outer region contained a reference core material of 15 v/o $U^{238}$, 15 v/o $U^{235}$, 15 v/o iron, and 55 v/o sodium.

In the first two problems, the Doppler element was thorium metal. Therefore the resonances in the two regions were at different energies. To determine the effect of the interference of these resonances, the first problem was run with resonances in both regions, and the second was run with the resonance cross sections in the outer region set equal to zero. As shown in Table VIII, the effect was very small. The fractional increase in the absorption rate of the Doppler element, per degree, was 6% higher with the interacting resonances present.

TABLE VIII. Effect of Surrounding Doppler Element by Material of Different Resonances

| Composition | | $\frac{1}{A_1}\frac{\partial A_1}{\partial T} \times 10^4$,* $^\circ K^{-1}$, |
|---|---|---|
| Region 1 | Region 2 | in Region 1 |
| Thorium (with resonances) | U-Na-Fe (with resonances) | 4.55 ± 0.09 |
| Thorium (with resonances) | U-Na-Fe (without resonances) | 4.20 ± 0.09 |
| Uranium (with resonances) | U-Na-Fe (with resonances) | 5.04 ± 0.10 |
| Uranium (with resonances) | U-Na-Fe (without resonances) | 2.69 ± 0.07 |

*A = absorption probability. The logarithmic derivative is the tabulated number times $10^{-4}$.

†J. R. Stehn et al., Neutron Cross Sections, Second Edition, Supplement No. 2, Volume III (Feb 1965).

2. Case 2: Doppler Element Surrounded by the Same Resonance Absorber

In the third and fourth problems, the Doppler element was uranium metal. Therefore the resonances in the two regions were at the same energies. The resulting interaction was found to be significant. The resonances in the outer region increased the Doppler effect in the uranium Doppler element by 87%.

3. Case 3: Interacting Materials Separated by Iron

Additional problems were run to determine the effect of the heater and the structural material separating the sample from the unheated core region. The interaction effect was significantly reduced when the interacting resonance materials were separated by iron. The amount of iron considered was equivalent to 1/16, 1/8, and 1/4 in. The presence of these iron cans reduces the interaction effect from 87 to 64, 56 and 30%, respectively, as shown in Table IX. The amount of iron present in the Argonne experiments was probably sufficient to prevent the detection of any interaction effect.

TABLE IX. Effect of Structural Material Separating Doppler Element and Surrounding Material with the Same Resonances

| Composition | | | $\frac{1}{A}\frac{\partial A}{\partial T} \times 10^4$,* $^\circ K^{-1}$, |
|---|---|---|---|
| Region 1 | Region 2 | Region 3 | in Region 1 |
| $U^{238}$ (with resonances) | Void | U-Na-Fe (without resonances) | 2.69 ± 0.07 |
| $U^{238}$ (with resonances) | Void | U-Na-Fe (with resonances) | 5.04 |
| $U^{238}$ (with resonances) | 1/16 in. Fe | U-Na-Fe (with resonances) | 4.40 |
| $U^{238}$ (with resonances) | 1/8 in. Fe | U-Na-Fe (with resonances) | 4.28 |
| $U^{238}$ (with resonances) | 1/4 in. Fe | U-Na-Fe (with resonances) | 3.51 |

*A = absorption probability. The logarithmic derivative is the tabulated number times $10^{-4}$.

4. Case 4: Variation of Interference Effect with Blanket Thickness

Additional problems were run to determine the optimum thickness of the blanket to produce the maximum interference effect. As shown by Table X, the optimum thickness is about 3/8 in. of thorium metal.

TABLE X. Variation of Interference Effect with Blanket Thickness

Region 1: Thorium Doppler element
Region 2: 1/16 in. iron
Region 3: Thorium blanket
Region 4: Uranium-sodium-iron core

| Blanket Thickness, in. | $\frac{1}{A}\frac{\partial A}{\partial T} \times 10^4$,* $°K^{-1}$, in Region 1 |
|---|---|
| 0 | -5.4 |
| 3/16 | -5.9 |
| 3/8 | -6.2 |
| 3/4 | -4.4 |

*A = absorption probability. The logarithmic derivative is the tabulated number times $10^{-4}$.

## C. Conclusions

The results given in Tables VIII-X lead to the following conclusions:

1. The presence of the unbroadened resonances in the "cold" surrounding material significantly increases the Doppler effect of the heated sample when the Doppler element and surroundings contain the same resonance absorber.

2. The Doppler effect of the heated sample is relatively insensitive to the presence of unbroadened resonances in the surroundings that are different from those of the sample.

3. The cold-hot interaction effect, which is closely analogous to the usual Dancoff effect, is extremely sensitive to the presence of the nonresonant scatterers surrounding the sample. The presence of a large amount of these nonresonant scatterers such as stainless steel tube and structure materials, which exist in almost all Doppler measurements, may substantially decrease the interaction effect discussed above.

# ACKNOWLEDGMENTS

The advice, encouragement, and assistance of many associates have contributed to the successful completion of this work. Of these, I mention the following for whose help I am extremely grateful.

I wish to thank Professor George H. Miley and Dr. Paul F. Gast for their guidance in the performance of this work and preparation of the thesis; Professor Marvin E. Wyman and Professor Arthur B. Chilton for several valuable technical and philosophical discussions; Dr. Richard N. Hwang and Dr. Henry C. Thacher for their assistance on some questions of reactor physics and mathematics; Dr. Robert Avery, Dr. Harry H. Hummel, Mr. Lyman J. Templin, and other members of staff of the Argonne National Laboratory for their personal help and for arranging the Ph.D. thesis appointment, under which this work was performed.

REFERENCES


1. C. Adkins, *Effects of Chemical Binding on the Doppler Broadened Cross Section of Uranium in a $UO_2$ Lattice*, Ph.D. thesis, Carnegie Institute of Technology, Pittsburgh, Pa. (1966).
2. G. Albert, "A General Theory of Stochastic Estimates of the Neumann Series for the Solution of Certain Fredholm Integral Equations and Related Series," *Symposium on Monte Carlo Methods*, H. A. Meyer, ed., pp. 37-46, Wiley, New York (1956).
3. E. Amaldi, O. D'Agostino, E. Fermi, B. Pontecorvo, F. Rasetti, and E. Segre, *Artificial Radioactivity Produced by Neutron Bombardment-II*, Proc. Roy. Soc. *A149*, 522 (1935).
4. W. Arnold, Jr., and R. Dannels, *A Monte Carlo Study of the Doppler Effect in $UO_2$ Fuel*, WCAP-1572 (1960).
5. J. Beardwood and J. Tyror, *Monte Carlo Calculations of Effective Resonance Integrals of $UO_2$ Rods*, AEEW-R-247 (1963).
6. G. Beck and L. Horsley, *Nonelastic Collision Cross Sections for Slow Neutrons*, Phys. Rev. *47*, 510 (1935).
7. S. Berberion, *Measure and Integration*, Macmillan, New York (1963).
8. M. Berger, *Reflection and Transmission of Gamma Radiation by Baniers: Monte Carlo Calculation by a Collision-Density Method*, J. Res. Nat. Bur. Stand. *55*, 343-350 (1955).
9. M. Berger and J. Doggett, *Reflection and Transmission of Gamma Radiation by Barriers: Semianalytic Monte Carlo Calculation*, J. Res. Nat. Bur. Stand. *56*, 89-98 (1956).
10. H. Bethe, *Theory of Disintegration of Nuclei by Neutrons*, Phys. Rev. *47*, 747 (1935).
11. H. Bethe and G. Placzek, *Resonance Effects in Nuclear Processes*, Phys. Rev. *51*, 450 (1937).
12. J. Blatt and V. Weisskopf, *Theoretical Nuclear Physics*, Wiley, New York (1952).
13. G. Breit, *Interpretation of Resonances in Nuclear Reactions*, Phys. Rev. *58*, 506 (1940).
14. G. Breit and E. Wigner, *Capture of Slow Neutrons*, Phys. Rev. *49*, 519 (1936).
15. N. Candelore and R. Gast, *Recap II - A Monte Carlo Program for Estimating Epithermal Capture Rates in Rod Arrays*, WAPD-TM-427 (1964).
16. T. Carleman, *Les Functions Quasi Analytiques*, Gauthier-Villars, Paris (1926).
17. S. G. Carpenter, L. A. Mountford, T. H. Springer, and R. J. Tuttle, "Dependence of the Doppler Coefficient of Reactivity for Heavy Elements on Chemical Form, Surface-to-Mass Ratio, and Neutron Spectrum," *Proceedings of the International Conference on Fast Critical Experiments and Their Analysis, October 10-13, 1966*, ANL-7320.

18. E. Cashwell and C. Everett, *A Practical Manual on the Monte Carlo Method for Random Walk Problems*, Pergamon Press, N. Y. (1959).

19. B. C. Ceruti, V. Lichtenberger, D. Okrent, R. E. Rice, Jr., and F. W. Thalgott, *ZPR-III, Argonne's Fast Critical Facility*, Nucl. Sci. Eng. *1*, 126 (1956).

20. J. Chernick, "Theory of Uranium-Water Lattices," *Proceedings of the First International Conference on Peaceful Uses of Atomic Energy, Geneva 5*, p. 215-228 (1956).

21. J. Chernick and R. Vernon, *Some Refinements in the Calculation of Resonance Integrals*, Nucl. Sci. Eng. *4*, 649-672 (1958).

22. A. B. Chilton, *A New Variant to the Exponential Transformation Technique in Monte Carlo Shielding Calculations*, Nucl. Sci. Eng. *24*, 200 (1966).

23. M. Clark, Jr., and K. Hansen, *Numerical Methods of Reactor Analysis*, Academic Press, N. Y. (1964).

24. N. Corngold, *Resonance Escape Probability in Slab Lattices*, BNL-445 (1956).

25. E. Creutz, H. Jupnik, T. Snyder, and E. Wigner, *Effect of Geometry on Resonance Absorption of Neutrons by Uranium*, J. Appl. Phys. *26*, 258 (1955).

26. A. V. Crewe *et al.*, *Reactor Development Program Progress Report, October 1964*, ANL-6965.

27. P. W. Davison *et al.*, *Microscopic Lattice Parameters in Single- and Multi-region Cores*, WCAP-1434 (1960).

28. J. Doob, *Stochastic Processes*, Wiley, New York (1953).

29. L. Dresner, *Resonance Absorption in Nuclear Reactors*, Pergamon Press, New York (1960).

30. R. Evans, *The Atomic Nucleus*, McGraw Hill, New York (1955).

31. E. Fermi and R. Richtmyer, *Note on Census-taking in Monte Carlo Calculations*, LADC-946 (1948).

32. H. Feshbach, D. Peaslee, and V. Weisskopf, *On the Scattering and Absorption of Particles by Atomic Nuclei*, Phys. Rev. *71*, 145 (1947).

33. G. Fischer, D. Meneley, R. Hwang, E. Groh, and C. Till, *Doppler Effect Measurements in Plutonium-Fueled Fast Power Breeder Reactor Spectra*, Nucl. Sci. Eng. *25*, 37-46 (1966).

34. F. Firk, J. Lynn, and M. Moxon, *Resonance Parameters of the Neutron Cross Section of U-238*, Nucl. Phys. *41*, 614 (1963).

35. D. Fraser, *Nonparametric Methods in Statistics*, Wiley, New York (1957).

36. D. Fraser, *Statistics: An Introduction*, Wiley, New York (1958).

37. T. C. Fry, *Probability and Its Engineering Uses* (Second Ed.), D. Van Nostrand Co., Princeton, N. J. (1965).

38. J. Garg, J. Rainwater, J. Petersen, and W. Havens, Jr., *Neutron Resonance Spectroscopy. III. Th-232 and U-238*, Phys. Rev. *134*, B985 (1964).

39. G. Goertzel and M. Kalos, "Monte Carlo Methods in Transport Problems," *Progress in Nuclear Energy; Phys. and Math.*, II, p. 315 (1958).

40. P. Greebler, B. Hutchins, and J. Sueoka, *Calculation of Doppler Coefficient and Other Safety Parameters for a Large Fast Oxide Reactor*, GEAP-3646 (1961).

41. P. Greebler and B. Hutchins, "The Doppler Effect in a Large Fast Reactor," *Proceedings of the Seminar on the Physics of Fast and Intermediate Reactors, Vienna, Austria, 1961*, Vol. III, 121, Int. Atom. Eng. Authority, Vienna (1962).

42. P. Greebler and E. Goldman, *Doppler Calculations for Large Fast Ceramic Reactors*, GEAP-4092 (1962).

43. S. Haber, *A Modified Monte-Carlo Quadrature*, Math. of Comp. *20*, No. 95, p. 361 (1966).

44. J. Hammersley, *Monte Carlo Methods*, Wiley, New York (1964).

45. C. Hastings, Jr., *Approximations for Digital Computers*, Princeton Univ. Press, Princeton, N. J. (1955).

46. H. Honeck, *Some Methods for Improving the Cylindrical Reflecting Boundary Condition in Cell Calculations of the Thermal Neutron Flux*, Trans. ANS *5*, No. 2 (1962).

47. T. Hull and R. Dobell, *Random Number Generators*, Soc. Indust. Appl. Math. Rev. *4*, 230 (1962).

48. H. Kahn, *Random Sampling (Monte Carlo) Techniques in Neutron Attenuation Problems*, Nucleonics *6*, 27-33, 36, 60-65 (1950).

49. H. Kahn and T. Harris, *Estimation of Particle Transmission by Random Sampling*, Nat. Bur. Stand. Appl. Math. Ser. *12*, 27-30 (1951).

50. H. Kahn and A. Marshall, *Methods of Reducing Sample Size in Monte Carlo Computations*, J. Oper. Res. Soc. Amer. *1*, 263-271 (1953).

51. H. Kahn, *Applications of Monte Carlo*, AECU-3259 (1954).

52. H. Kahn, "Use of Different Monte Carlo Sampling Techniques," *Symposium on Monte Carlo Methods*, pp. 146-190, Wiley, New York (1956).

53. P. Kapur and R. Peierls, *The Dispersion Formula for Nuclear Reactions*, Proc. Roy. Soc. *A166*, 277 (1938).

54. M. Kendal and B. Smith, *Random Sampling Numbers*, Tracts for Computers *24*, Cambridge Univ. Press, London (1939).

55. P. Kier, *The Effect of a Non-asymptotic Neutron Source on Resonance Absorption in Slab Lattices*, Ph.D. thesis, Massachusetts Institute of Technology (1963).

56. P. H. Kier, *RIFF RAFF, A Program for Computation of Resonance Integrals in a Two-region Cell*, ANL-7033 (1965).

57. P. Kier, "A Method of Computing Resonance Integrals in Multiregion Reactor Cells," *International Conference on the Utilization of Research Reactors and Reactor Mathematics and Computation*, Mexico, D.F. (1967).

58. W. Lamb, *Capture of Neutrons by Atoms in a Crystal*, Phys. Rev. *55*, 190 (1939).

59. D. Leslie, J. Hill, and A. Jonsson, *Improvements in the Theory of Resonance Escape in Heterogeneous Fuel*, AEEW-R353 (1964).

60. E. Lewis, *A Boltzmann Integral Equation Treatment of Resonance Absorption in Reactor Lattices*, Ph.D. thesis, University of Illinois (1965).

61. L. E. Link *et al.*, *1000-MW(e) Metal-fueled Fast Breeder Reactor*, ANL-7001 (June 1966).

62. R. Meghreblian and D. Holmes, *Reactor Analysis*, McGraw-Hill, New York (1960).

63. M. McNelly *et al.*, *Liquid Metal Fast Breeder Reactor Design Study*, GEAP-4418 (1964).

64. R. von Mises, edited by Hilda Guringer, *Mathematical Theory of Problems and Statistics*, Academic Press, N. Y. (1964).

65. U. Möller, *Unterprogramme zur Lösung Neutronenphysikalisher Probleme Mit Hilfe der Monte-Carlo-Method*, KFK-298, Institut für Neutronenphysik und Reaktortechnik Kernsforschungszentrum, Karlsruhe (1965).

66. P. Moon and J. Tillman, Nature *135*, 904 (1935).

67. K. Morton, "Calculation of Resonance Escape Probability by Monte Carlo Methods," *Proc. 2nd Int. Conf. PUAE 16*, 187 (1958).

68. R. Nicholson, *Doppler Effect in Fast Reactors*, APDA-139 (1960).

69. L. Nordheim, *A Program of Research and Calculation of Resonance Absorption*, GA-2527 (1961).

70. L. Nordheim, *A New Calculation of Resonance Integrals*, Nucl. Sci. Eng. *12*, 457-463 (1962).

71. J. Olhoeft, *The Doppler Effect for a Non-uniform Temperature Distribution in Reactor Fuel Elements*, Ph.D. thesis, The University of Michigan (1963).

72. D. O'Shea and H. Thacher, *Computation of Resonance Line Shape Functions*, Trans. ANS *6*, No. 1, 36-37 (1963).

73. C. Porter and R. Thomas, *Fluctuations of Nuclear Reaction Widths*, Phys. Rev. *104*, 483-489 (1956).

74. A. L. Rago and H. H. Hummel, *ELMOE: An IBM-704 Program Treating Elastic Scattering Resonances in Fast Reactors*, ANL-6805 (Jan 1964).

75. J. Rainwater, *Handbuch der Physic*, edited by S. Flügge, Vol. 40, Springer-Verlag, Berlin (1957).

76. O. Rice, *Perturbations in Molecules and the Theory of Predissociation and Diffuse Spectra*, Phys. Rev. *33*, 748 (1929).

77. R. D. Richtmyer, "Resonance Capture Calculations for Lattices by the Monte-Carlo Method," *Proceedings of the Brookhaven Conference on Resonance Absorption of Neutrons in Nuclear Reactors, Brookhaven*, pp. 82-89 (1956).

78. R. Richtmyer, R. Van Norton, and A. Wolfe, "Monte Carlo Calculations of Resonance Capture in Reactor Lattices," *Proceedings of the 2nd International Conference PUAE 16*, 180 (1958).

79. G. Roe, *The Absorption of Neutrons in Doppler Broadened Resonances*, KAPL-1241 (1954).

80. J. Rosen *et al.*, *Slow Neutron Resonance Spectroscopy, I:* $U^{238}$, Phys. Rev. *118*, No. 3 (1960).

81. W. Rothenstein and D. Tabak, *Philco 2000 Code for the Calculation of Resonance Escape Probability in Heterogeneous Reactors by the Monte Carlo Method*, UC-32-3; IA-1001, Israel Atomic Energy Commission, Yavne (1965).

82. R. Sachs, *Nuclear Theory*, Addison-Wesley, Cambridge, Mass. (1953).

83. J. Spanier, *Monte Carlo Methods and Their Application to Neutron Transport Problems*, WAPD-195 (1959).

84. R. B. Stick *et al.*, *Liquid Metal Fast Breeder Reactor Design Study*, WCAP-3251-1 (1964).

85. N. Steen, *A Simple Method to Improve the Efficiency of the* $\Sigma_a/\Sigma_T$ *Estimator in Monte Carlo Programs*, Trans. ANS *9*, No. 1, 204 (1966).

86. F. Storrer, A. Khairallah, and J. Ozeroff, "Measurements of the Doppler Coefficient in Large Fast Power Reactors Using a Fast Critical Assembly and an Experimental Fast Reactor; Part I. Theoretical Aspects of the Measurement of the Doppler Coefficient in a Critical Facility," *Proceedings of the Conference on Breeding, Economics, and Safety in Large Fast Power Reactors, October 7-10, 1963*, ANL-6792 (Dec 1963).

87. L. Szilard, Nature *136*, 950 (1935).

88. J. Tait, *An Introduction to Neutron Transport Theory*, Longman's, Green, and Co., Ltd., London (1964).

89. L. J. Templin, ed., *Reactor Physics Constants, Second Edition*, ANL-5800 (July 1963).

90. T. Tiechman, *Some General Properties of Nuclear Reaction and Scattering Cross Sections*, Phys. Rev. *77*, 506 (1950).

91. C. E. Till, R. A. Lewis, and E. F. Groh, *Doppler Effect Measurements on a Dilute Fast-Carbide Assembly, ZPR-6 Assembly 4Z*, Trans. ANS *8*, No.2 (1965).

92. S. Ulam, "On the Monte Carlo Method," *Proceedings of the Second Symposium on Large-scale Digital Calculating Machinery*, pp. 207-212 (1951).

93. S. Visner *et al.*, *Liquid Metal Fast Breeder Reactor Design Study*, CEND-200 (1964).

94. H. Wall, *Analytic Theory of Continued Fractions*, Van Nostrand, N. Y. (1948).

95. E. Wigner, *Results and Theory of Resonance Absorption*, ORNL-2309, p. 59, Conference on Neutron Physics by Time of Flight, Gatlinburg (1956).

96. E. Wigner, *On the Behavior of Cross Sections Near Thresholds*, Phys. Rev. *73*, 1002 (1948).

97. E. Wigner, *Proceedings of Symposia in Applied Math, New York, 1958, 11*, Am. Math. Soc., Providence (1961).

98. E. Wigner, E. Creutz, H. Jupnik, and T. Snyder, *Resonance Absorption of Neutrons in Spheres*, J. Appl. Phys. *26*, 260 (1955).

99. E. Wigner and L. Eisenbud, *Higher Angular Momenta and Long Range Interaction in Resonance Reactions*, Phys. Rev. *72*, 29 (1947).

100. E. R. Woodcock, T. Murphy, P. J. Hemmings, and T. C. Longworth, "Techniques Used in the GEM Code for Monte Carlo Neutronics Calculations in Reactors and Other Systems of Complex Geometry," *Proceedings of the Conference on the Application of Computing Methods to Reactor Problems, May 17-19, 1965*, ANL-7050 (Aug 1965).

101. C. Zerby, *A Monte Carlo Calculation of the Response of Gamma-ray Scintillation Counters*, Methods in Computational Physics *1*, pp. 89-133 (1963).